FD-RAN Empowered Multiple Base Stations Cooperative ISAC for Low-Altitude Networks

Jianzhe Xue, *Graduate Student Member, IEEE*, Haibo Zhou, *Fellow, IEEE*, Haohai Huang, *Student Member, IEEE*, Gui Wen, *Student Member, IEEE*, Yunting Xu, *Member, IEEE*, Xinyu Huang, *Member, IEEE*, and Xuemin Shen, *Fellow, IEEE*

***Abstract*—The fully-decoupled radio access network (FD-RAN) with multiple base stations (BS) networked cooperation is expected to provide high-quality communication coverage for aerial vehicles while sensing their locations accurately and efficiently. In this paper, we propose a novel multiple BSs cooperative passive integrated sensing and communication (ISAC) framework in FD-RAN for low-altitude aerial vehicles. It utilizes the Doppler shift information from uplink orthogonal frequency division multiplexing (OFDM) signals to achieve efficient localization without incurring additional sensing overhead. Specifically, the carrier frequency offset (CFO) compensation process at each BS captures Doppler shift resulting from the relative motion between the aerial vehicle and the BS. Considering the position and velocity of the aerial vehicle as unknown variables, the localization is achieved by formulating and solving a system of equations describing these Doppler shifts. Furthermore, to enable accurate trajectory tracking, we design a learning-based adaptive double-filter (LADF) algorithm, which leverages temporal correlations in both Doppler shift measurements and vehicle trajectories to improve the time-continuous localization. Extensive simulation results demonstrate the effectiveness of our proposed ISAC framework in low-altitude FD-RAN, which can enhance the coverage performance and efficiently provide accurate localization for aerial vehicles.**

***Index Terms*—Low-altitude, ISAC, cooperative, Doppler shift, deep learning.**

I. Introduction

LOW-ALTITUDE aerial vehicles, which include electric vertical take-off and landing (eVTOL), uncrewed aerial vehicles (UAV), and crewed aerial vehicles, are essential to the rapidly growing low-altitude economy [1], [2], [3], [4], [5], [6]. Operating in such dynamic and congested airspaces, aerial vehicles necessitate advanced capabilities for real-time data exchange and accurate positioning and navigation to ensure safe flight operations [7], [8], [9], [10], [11]. In addition, the position information of the aerial vehicle is crucial for beamforming, which can further improve the communication performance [12], [13]. However, frequent reporting of location information by vehicles consumes bandwidth, while some may even be reluctant to share it. Therefore, the low-altitude network needs the sensing ability to support both navigation and communication services. Traditional systems that manage sensing and communication separately often face significant challenges, including increased latency, higher energy consumption, and inefficient spectrum utilization. These issues can severely impede the performance and scalability of aerial vehicle operations, thereby limiting their potential impact on the low-altitude economy.

To meet these critical demands, integrated sensing and communication (ISAC) has emerged as a pivotal technology that seamlessly combines wireless communication and sensing functions within a single system [14], [15], [16], [17], [18], [19]. This integrated approach enables the sharing of hardware resources, spectrum, and signal processing techniques, thereby enhancing overall performance and resource efficiency while reducing deployment costs. Most traditional ISAC implementations rely on a single base station (BS) architecture, where both communication and sensing functions are confined to a single cell. Although single BS ISAC provides foundational integration, it is limited in terms of sensing coverage and resolution. To address these limitations, multiple BSs cooperative ISAC leverages the collaboration of several BSs distributed across different locations, thereby expanding coverage and enhancing both communication and sensing capabilities [20], [21]. By pooling signals from multiple BSs, multi-BS cooperative ISAC offers higher reliability, improved resource efficiency, and enhanced sensing accuracy compared to single BS ISAC.

A promising implementation of multiple BSs cooperative ISAC is based on Doppler shift analysis, which is particularly well-suited for low-altitude aerial vehicles. Fast-moving aerial vehicles experience significant relative motion with respect to ground BSs, resulting in Doppler shifts in the communication signals [22], [23], [24], [25], [26], [27], [28]. In an uplink orthogonal frequency division multiplexing (OFDM) communication system with joint reception by multiple BSs, each BS first estimates and compensates for the carrier frequency offset (CFO) using the cyclic prefix (CP). This CFO compensation

Received 22 September 2025; revised 14 January 2026; accepted 6 February 2026. Date of publication 10 February 2026; date of current version 26 February 2026. This work was supported by the National Natural Science Foundation of China under Grant 62271244. Recommended for acceptance by Dr. Weijie Yuan. *(Corresponding author: Haibo Zhou.)*

Jianzhe Xue, Haibo Zhou, Haohai Huang, and Gui Wen are with the School of Electronic Science and Engineering, Nanjing University, Nanjing 210023, China (e-mail: jianzhexue@smail.nju.edu.cn; haibozhou@nju.edu.cn; haohaihuang@smail.nju.edu.cn; weng5@chinaunicom.cn).

Yunting Xu is with the School of Computer Science and Engineering, Nanyang Technological University, Singapore 639798 (e-mail: yunting.xu@ntu.edu.sg).

Xinyu Huang and Xuemin Shen are with the Department of Electrical and Computer Engineering, University of Waterloo, Waterloo, ON N2L 3G1, Canada (e-mail: x357huan@uwaterloo.ca; sshen@uwaterloo.ca).

Digital Object Identifier 10.1109/TNSE.2026.3663391

process inherently accounts for the Doppler shift caused by the relative motion between the eVTOL and each BS [29], [30], [31]. The Doppler shift observed at each BS can be mathematically modeled as a set of equations, where the speed and position of the aerial vehicle are the unknown variables [32], [33], [34]. By solving this system of equations, the position of the aerial vehicle can be accurately determined, thereby enabling effective localization and tracking within passive ISAC systems.

Moreover, multiple BSs cooperative passive ISAC based on Doppler shift offers significant advantages in spectrum utilization and robustness to noise. Unlike schemes relying on dedicated sensing signals, which require allocating part of the limited communication time-frequency resources exclusively to sensing, the Doppler-based cooperative ISAC approach leverages existing communication signals without necessitating additional time-frequency overhead [35]. This efficient spectrum usage allows the same bandwidth to support data transmission and sensing simultaneously. Furthermore, compared to radar-like sensing methods that rely on analyzing echo signals reflected from targets, the Doppler-based approach inherently benefits from the accurate estimation of CFO in OFDM systems. Since accurate CFO estimation is essential for maintaining communication performance, the estimated Doppler shifts from these signals provide a more robust sensing approach, enhancing resilience against noise and interference. In addition, the fully decoupled radio access network (FD-RAN), as a new sixth-generation (6G) architecture, can economically support dense deployment of uplink BSs via uplink–downlink decoupling, enabling close real-time cooperation among uplink BSs [36], [37]. FD-RAN enables the network to aggregate Doppler shift measurements from multiple BSs in real time by implementing efficient data fusion and information exchange for the joint processing of multiple uplink BSs. The densely deployed uplink BS and efficient multi-BS collaboration capabilities in FD-RAN provide a solid foundation for the cooperative ISAC system.

Trajectory tracking of aerial vehicles is a critical requirement in the low-altitude economy, necessitating time-continuous localization that can be significantly improved by leveraging temporal correlations [38], [39], [40]. Although noise in the uplink signal introduces errors in Doppler shift estimation, the relative motion between aerial vehicles and BSs evolves continuously and smoothly over time, rendering Doppler shift variations largely predictable. This predictability can be effectively captured using deep learning techniques, which exploit the temporal correlations in Doppler shift dynamics to provide more accurate real-time estimates [41], [42], [43], [44], [45], [46]. Furthermore, since the speed and trajectory changes of aerial vehicles adhere to fundamental kinematic principles, additional refinements in time-continuous localization can be achieved through techniques such as Kalman filtering. By separately utilizing temporal correlations and filtering Doppler shifts and trajectory data, the accuracy of trajectory tracking is significantly enhanced [47]. Consequently, Doppler shift based ISAC systems are exceptionally well-suited to meet the stringent demands of trajectory tracking for high-mobility aerial vehicles, thereby ensuring reliable and efficient operation in complex low-altitude environments.

In this paper, we present a novel multiple BSs cooperative passive ISAC framework for low-altitude aerial vehicles. By leveraging Doppler shift analysis, our approach eliminates the need for additional sensing resources, thereby reducing overhead while maintaining robust localization capabilities. Specifically, in the uplink communication module, each FD-RAN uplink BS independently estimates and compensates for the Doppler shift. The compensated signals from all participating BSs are then combined using a maximum ratio combination (MRC) algorithm, improving the communication performance. Additionally, we propose a Doppler shift-based localization method for aerial vehicles that utilizes Doppler estimations inherently provided by OFDM receivers, thereby avoiding the consumption of additional resources. Furthermore, by exploiting the temporal correlation between Doppler shifts and trajectory data in trajectory-tracking applications, we introduce a learning-based approach to enhance the accuracy of continuous-time localization. Finally, we demonstrate the superior performance of our multiple BSs cooperative ISAC framework through extensive simulations. The primary contributions of this work can be summarized as follows:

- We propose a multiple BSs cooperative passive ISAC framework for low-altitude aerial vehicles, leveraging Doppler shifts inherently obtained from OFDM systems for localization, eliminating the need for additional sensing resources.
- We formulate the Doppler shift-based aerial vehicle localization problem under noise condition in the ISAC system as a minimization-of-error task, and propose a localization solution based on the nonlinear least squares algorithm.
- We design a learning-based adaptive double filter (LADF) algorithm for time-continuous localization of aerial vehicles, exploiting temporal correlations in both Doppler shift and trajectory data to improve the accuracy of trajectory tracking.

The remainder of this paper is organized as follows. Section II reviews related works on low-altitude ISAC, multi-BS cooperative ISAC, and Doppler shift based localization. Section III presents the system model and the proposed ISAC framework. Section IV formulates the localization problem and provides a solution for single time slot localization. Section V presents the proposed LADF algorithm for time-continuous localization. Finally, Section VI shows the simulation results, followed by the conclusion in Section VII.

II. Related Work

A. Low-Altitude Economy With ISAC

Low-altitude aerial vehicles, typically referring to small- and medium-sized platforms operating at altitudes below 3 km, are at the core of the rapid expansion of the low-altitude economy [54]. Their deployment spans a wide range of applications, including cargo delivery, aerial inspection, emergency response, and urban transportation. Compared with traditional aviation, low-altitude economy operations are characterized by high density, frequent trajectory changes, and heterogeneous service demands, all

TABLE I
THE SUMMARY OF TYPICAL COOPERATIVE ISAC ARCHITECTURES

Signal	Ref.	Scenario	Summary
Dedicated radar signals	[48]	Each BS transmits a signal and receives its own echo signal.	(a) The location and velocity of the UAV are estimated by fusing sensing information from multiple BSs. (b) The weighted sum of secrecy rate and radar mutual information rate is maximized to balance sensing and security.
	[49]	Every BS transmits a signal and receives echo signals.	(a) A networked ISAC scheme based on multi-point coordinated joint transmission and distributed MIMO radar techniques is proposed. (b) There is no correlation between the communication signal and the radar signal.
Downlink OFDM	[50]	One primary BS transmits sensing signals, while both the primary BS and two secondary BSs capture the echo signals.	(a) The centralized extended Kalman filter (EKF) is used to fuse estimates from the three BSs, and prediction is leveraged for tracking. (b) The primary BS handover strategy is proposed to select the optimal BS from the three BSs as the new PBS in real-time.
	[51]	One BS transmits a signal, multiple BSs receive echo signals.	(a) The scattering characteristics of targets in a cooperative sensing scenario are analyzed. (b) A multi-node signal-level data fusion method is proposed to improve sensing accuracy through joint processing.
Downlink OTFS	[52]	Multiple BSs transmit signals, multiple BSs receive signals.	(a) The cell-free ISAC system model with multi-antenna access points (APs) is developed based on the OTFS signal. (b) The downlink spectral efficiency expression is derived regarding multi-antenna APs and optional sensing beams.
Uplink OFDM	[53]	Multiple UEs transmit signals, targets reflect signals, multiple BSs receive signals.	(a) An interference analysis framework considering the mutual interference among ISAC UEs and the communication UEs' interference is presented. (b) A resource management scheme is proposed to enhance cooperative sensing performance.
	Our	The aerial vehicle transmits uplink signal, multiple BSs extract Doppler shifts from the received signals.	(a) A Doppler shift-based localization method within a multi-BS cooperative passive ISAC framework is proposed. (b) A learning-based adaptive filtering approach for accurate trajectory tracking of aerial vehicles is designed.

within congested and dynamic airspaces [55]. These unique features place stringent requirements on wireless networks to provide continuous connectivity, precise localization, and robust coordination capabilities.

Meeting these requirements with conventional wireless systems remains challenging [56], [57], [58], [59]. On the one hand, schemes that depend on periodic position reporting from aerial vehicles lead to excessive signaling overhead and may struggle to keep pace with highly mobile and large-scale deployments. On the other hand, maintaining communication and sensing as independent subsystems results in duplicated infrastructure, inefficient spectrum usage, and higher energy consumption, which are impractical for future large-scale low-altitude economy scenarios.

These limitations have stimulated increasing interest in ISAC as a unified solution [60], [61], [62], [63], [64], [65]. ISAC exploits communication signals for both data exchange and perception tasks, thereby eliminating redundant signaling while enabling accurate trajectory tracking and situational awareness. Moreover, some works about the integration of sensing, communication, and computation have also been studied [66], [67]. Besides, the use of generative AI for ISAC has also been studied [68], [69], [70]. In the context of low-altitude economy, this integration is not only a matter of improving spectral efficiency, but also a prerequisite for ensuring safe airspace management, collision avoidance, and high-quality service delivery [71], [72], [73], [74]. Consequently, ISAC is widely viewed as a fundamental enabler for the sustainable development of low-altitude networks.

TABLE II
SIMULATION PARAMETERS

Parameter	Value
Radius of the hexagonal cell	200 m
aerial vehicle trajectory radius	400 m
BS antenna height	20 m
aerial vehicle speed	20 m/s
aerial vehicle transmit power	20 dBm
Carrier frequency	3 GHz
Bandwidth of each subcarrier	15 kHz
Number of OFDM subcarriers	72
CP length	18
Noise power	-114 dBm

B. Multi-BS Cooperative ISAC

Multiple BSs cooperative ISAC systems exploit the collaboration among distributed BSs to enhance target localization accuracy and communication performance, thereby overcoming the inherent limitations of single-BS setups [75], [76], [77]. Through multi-node cooperative perception and sensing data sharing, these systems enable wider coverage, improved robustness, and more efficient utilization of network resources.

A variety of architectures for multi-BS cooperative ISAC have been investigated in the literature. Radar-style designs allow each BS to transmit orthogonal or dedicated sensing signals and process its own echoes independently [48], [49]. Communication-oriented designs, on the other hand, employ downlink waveforms such as OFDM or OTFS, where one or multiple BSs transmit and multiple BSs jointly process the

received echoes [50], [51], [52]. More recently, uplink-based approaches have been explored, where multiple UEs transmit OFDM signals and distributed BSs collect the reflected echoes for joint sensing [53].

Beyond architectural designs, several works have further analyzed or validated the performance of cooperative ISAC [78], [79], [80], [81]. A networking-based ISAC hardware testbed that enhances cooperative perception is presented, achieving a 61% reduction in localization error compared to a single ISAC system [82]. The performance of cooperative ISAC is analyzed, revealing that deploying N transceivers enhances cooperative sensing performance according to the $ln^2 N$ scaling law, while optimizing communication rates and cluster sizes to balance sensing and communication performance effectively [49]. A multiple BSs cooperative UAV sensing method using a MUSIC-based symbol-level fusion approach is studied for position and velocity estimation [83]. A fairness-based resource allocation framework that prioritizes the weakest links by maximizing the minimum radar sensing signal-to-interference-plus-noise ratio (SINR) is proposed for UAV detection [84]. The balance between sensing accuracy and additional cost is studied with Cramer-Rao bound (CRB) [85]. Moreover, ISAC based on cell free network architecture has also been studied from different aspects [86], [87], [88], [89].

Nevertheless, most of these designs rely on active echo-based sensing or additional downlink signaling, which inevitably consume extra spectrum and increase system overhead. In contrast, the FD-RAN enables dense deployment of low-cost uplink BSs with close cooperation [13], [36], offering a foundation for passive ISAC frameworks that exploit Doppler shifts in uplink OFDM transmissions without extra sensing signals.

C. Doppler Shift Based Localization

Doppler shift based localization involves estimating the position and velocity of a moving target using Doppler shift measurements from a group of stationary sensors, which can also be BSs in ISAC systems [90], [91], [92], [93], [94], [95]. The minimum number of Doppler shift measurements of echo signals required for finite and unique solutions in a two-dimensional (2D) scenario is derived, in which the importance of sensor placement is also discussed [32]. For the case of the signal emitted by the target, a 2D moving target is localized by observing the Doppler shift of the emitted signal from the target with the proposed constrained optimization methods, addressing errors in frequency and sensor positions, and validating accuracy under Gaussian noise [96].

Beyond these 2D localization studies, Doppler shift based localization has been further extended and generalized to more complex scenarios. The similar localization problem is expanded into a three-dimensional (3D) scenario and solved by two algorithms specially designed to address the complicated non-linear relation between the target location parameters and the observations [33]. A semi-definite programming solution is proposed for target localization that incorporates sensor motion effects on time delay and Doppler shift, which transforms a constrained weighted least squares problem into a convex programming problem [97]. The mobile source localization problem using time of arrival (TOA) and Doppler shift measurements is studied, which is formulated as a weighted least squares problem [98]. The problem of multi-target detection and tracking over a network of separately located Doppler shift measuring sensors is solved by using the probability hypothesis density (PHD) filter [99]. Moreover, the optimal sensor placement problem for stationary target localization by multiple moving Doppler-shift radars is considered and a solution based on maximizing the determinant of the Fisher information matrix is proposed and analyzed [100].

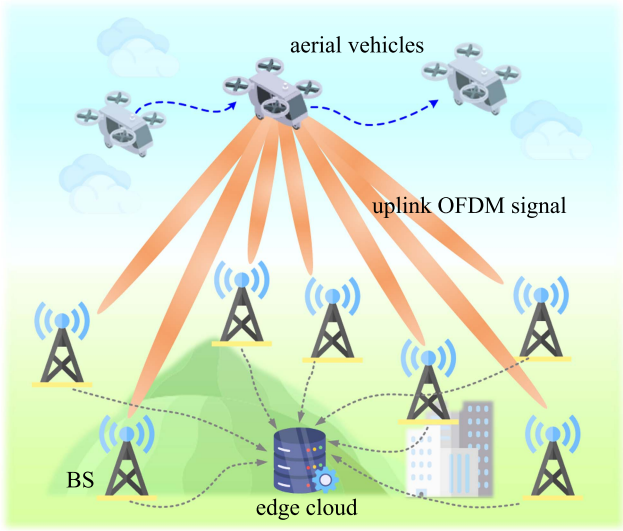

Fig. 1. Low-altitude ISAC scenario with uplink FD-RAN.

Compared with existing works in multiple BSs cooperative ISAC, we propose a novel passive sensing approach based on Doppler shift information. Moreover, we propose a learning-based approach for Doppler shift based time-continuous localization by leveraging the temporal correlations.

III. System Model

In this section, we first describe the low-altitude ISAC scenario, and the CP-based CFO estimation and compensation for the OFDM signal. Then, we present the multiple BSs cooperative ISAC framework, as well as the MRC joint decoding method for its communication module.

A. Scenario Description

We consider the ISAC system for a low-altitude aerial vehicle served by a group of ground uplink FD-RAN BSs. For notational simplicity and consistency, these entities are hereafter referred to as uplink BSs, or simply BSs when the context is clear. As shown in Fig. 1, the aerial vehicle operates in low-altitude airspace at a certain speed, and transmits uplink OFDM signals to multiple BSs. These BSs are connected to an edge cloud for cooperation, expecting to provide high-capacity communication services while simultaneously sensing the position of the aerial vehicle. They are denoted as $b = 1, \ldots, K$, where K represents

the total number of BSs. For the uplink OFDM signal consisting of M subcarriers, the frequency-domain OFDM symbol is denoted as $X(m), m = 0, \ldots, M-1$. Then, its time-domain OFDM signal can be further obtained by applying an M-point inverse discrete Fourier transform as,

$$x(n) = \frac{1}{\sqrt{M}} \sum_{m=0}^{M-1} X(m) e^{j\frac{2\pi mn}{M}}, \quad n = 0, \ldots, M-1, \quad (1)$$

where n denotes the discrete-time index for the time-domain samples of the time-domain OFDM signal. Furthermore, to eliminate inter-symbol interference, the cyclic prefix (CP) of length N_{C} is appended to the front of the time-domain OFDM signal, and then the time domain CP-OFDM signal is obtained as,

$$x_{\mathrm{C}}(n) = \begin{cases} x(n + M - N_{\mathrm{C}}), & n = 0, \ldots, N_{\mathrm{C}} - 1 \\ x(n - N_{\mathrm{C}}), & n = N_{\mathrm{C}}, \ldots, M + N_{\mathrm{C}} - 1 \end{cases}. \quad (2)$$

The CP, which is a copy of the last N_{C} samples of the OFDM symbol, ensures that linear convolution within the channel appears as circular convolution at the receiver, thus preserving the subcarrier orthogonality.

The aerial vehicle broadcasts this time domain CP-OFDM signal and each BS receives a distinct signal due to its unique position and the associated channel characteristics. Considering that low-altitude aerial vehicles are generally above the majority of ground-level obstructions, such as buildings, trees, and terrain features, their uncluttered space provides a cleaner environment for radio waves to propagate without being disrupted, and thus usually form the line-of-sight (LOS) channel between the aerial vehicle and the BSs [101]. Specifically, the time-varying complex channel gain of b-th BS is denoted as,

$$h^{(b)}(n) = |h^{(b)}| e^{j\theta^{(b)}} e^{j2\pi f^{(b)} n T_s}, \quad (3)$$

where $|h^{(b)}|$ is the gain amplitude and $e^{j\theta^{(b)}}$ is the initial phase response, $f^{(b)}$ is frequency shift, T_s is the system sampling period, and the exponential term $e^{j2\pi f^{(b)} n T_s}$ models the gradual phase rotation over time caused by the frequency shift. Within one OFDM symbol duration, the channel amplitude and Doppler shift are assumed quasi-static. Ignoring the small differences caused by inconsistencies in the clocks used for transceivers, this frequency shift consists mainly of the Doppler shift generated by the relative motion of the aerial vehicle towards or away from b-th BS. Since the relative velocities between the aerial vehicle and each BS are different, $f^{(b)}$ is also different between each BS, which implies that each BS observes a different Doppler shift. Then, the received time-domain CP-OFDM signal at b-th BS is obtained as,

$$r_{\mathrm{C}}^{(b)}(n) = h^{(b)}(n) x_{\mathrm{C}}(n) + w^{(b)}(n), \quad n = 0, \ldots, M + N_{\mathrm{C}} - 1, \quad (4)$$

where $w^{(b)}(n)$ is the Gaussian noise.

In the case of the LOS channel between the aerial vehicle and BSs, the received time-domain OFDM signal at the b-th BS after removing the CP can be expressed as,

$$\begin{aligned} r^{(b)}(n) &= r_{\mathrm{C}}^{(b)}(n + N_{\mathrm{C}}) \\ &= |h^{(b)}| e^{j\theta^{(b)}} e^{j2\pi f^{(b)}(n+N_{\mathrm{C}})T_s} x_{\mathrm{C}}(n + N_{\mathrm{C}}) \\ &\quad + w^{(b)}(n + N_{\mathrm{C}}), \end{aligned} \quad (5)$$

where $n = 0, \ldots, M-1$ is the discrete-time index for the time domain OFDM signal.

B. Doppler Shift Estimation and Compensation

The estimation and compensation of Doppler shift leverage the structural similarity between the CP and its corresponding segment in the main OFDM signal. In the transmitted time-domain CP-OFDM signal, the CP samples are a replica of a specific portion from the end of the OFDM symbol. However, when a Doppler shift is introduced by the wireless channel, it induces a CFO, resulting in a phase rotation of each sample in the received signal. This phase rotation disrupts the alignment between the CP and its corresponding segment, introducing a measurable phase difference. By analyzing this phase difference, the BS can accurately estimate and compensate for the Doppler shift, thereby mitigating its impact on signal integrity.

The correlation metric is a widely used measure of similarity between two signals and serves as a fundamental tool for CFO estimation in CP-OFDM systems. For the b-th BS, the correlation metric $R^{(b)}$ is defined as,

$$R^{(b)} = \sum_{n=0}^{N_{\mathrm{C}-1}} r_{\mathrm{C}}^{(b)*}(n) r_{\mathrm{C}}^{(b)}(n + M), \quad (6)$$

where $r_{\mathrm{C}}^{(b)*}(n)$ is the complex conjugate of $r_{\mathrm{C}}^{(b)}(n)$. This metric captures the phase offset caused by the Doppler shift between the CP and its corresponding tail segment in the time-domain OFDM signal. The angle of the correlation metric, $\angle(R^{(b)})$, represents the phase difference induced by the Doppler shift. It is directly related to the Doppler shift, and their relationship can be expressed as,

$$\angle(R^{(b)}) = 2\pi f^{(b)} M T_s. \quad (7)$$

By solving for $f^{(b)}$, the Doppler shift can be estimated as,

$$\hat{f}^{(b)} = \frac{\angle(R^{(b)})}{2\pi M T_s}. \quad (8)$$

The length of the correlation summation N_C affects the estimation variance, while the time interval corresponding to the phase difference is determined by the index interval M between the CP and the tail portion. This relationship provides a simple and direct method for Doppler shift estimation based on the phase of the correlation metric in CP-OFDM systems.

To mitigate the impact of the CFO on the received signal, phase compensation is applied to the time-domain OFDM signal $r^{(b)}(n)$. After Doppler compensation, the corrected received signal $\tilde{r}^{(b)}(n)$ can be expressed as,

$$\tilde{r}^{(b)}(n) = r^{(b)}(n) e^{-j2\pi \hat{f}^{(b)}(n+N_{\mathrm{C}})T_s}, \quad n = 0, \ldots, M-1. \quad (9)$$

where the exponential term $e^{-j2\pi \hat{f}^{(b)}(n+N_{\mathrm{C}})T_s}$ represents the phase compensation factor, designed to counteract the phase

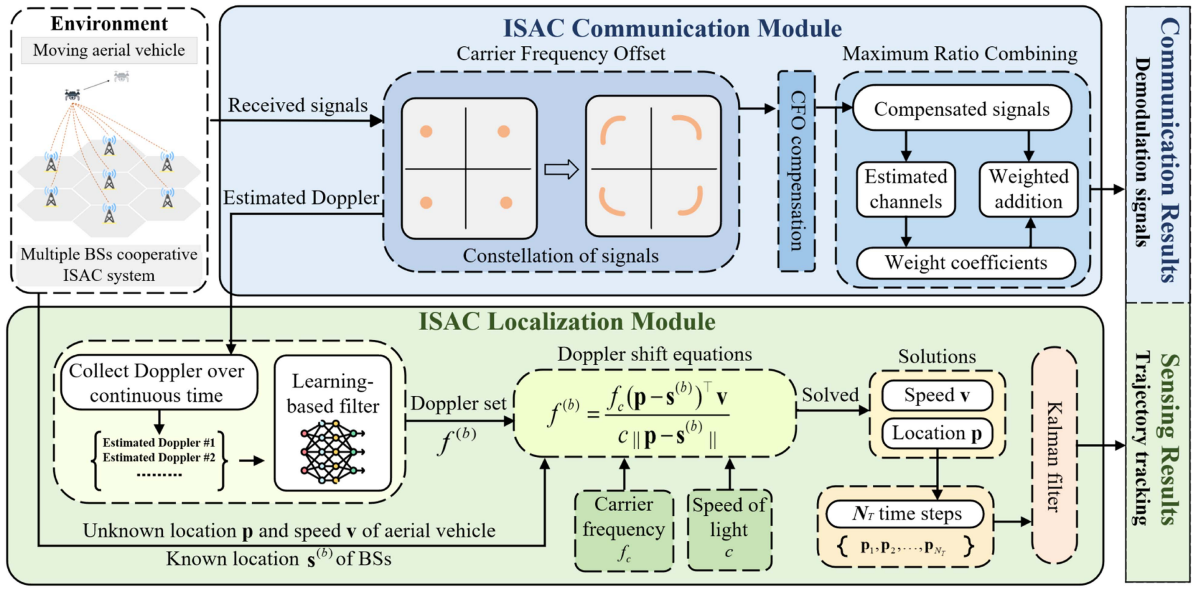

Fig. 2. Multiple BSs cooperative ISAC framework for low-altitude aerial vehicles.

rotation introduced by the Doppler shift. This approximation, treating the Doppler shift as a common phase rotation within an OFDM symbol, is valid when $|f^{(b)}| \ll \Delta f$, where Δf is the subcarrier spacing. By substituting the expression for $r^{(b)}(n)$ from (5) into (9), the compensated signal becomes,

$$\tilde{r}^{(b)}(n) = r_{\mathrm{C}}^{(b)}(n+N_{\mathrm{C}})e^{-j2\pi\hat{f}^{(b)}(n+N_{\mathrm{C}})T_s}, \quad n=0,\ldots,M-1. \tag{10}$$

After Doppler compensation, the Doppler-induced phase rotation in the signal $\tilde{r}^{(b)}(n)$ is largely mitigated. This recovered signal can then be processed by subsequent communication modules for demodulation and further signal analysis.

This process is necessary in OFDM communication systems to ensure that the distortion due to the Doppler shift is effectively reduced and the integrity of the transmitted information is maintained. Notably, it simultaneously and naturally provides the estimation of the Doppler shifts without adding additional overhead, which makes Doppler shift based localization possible and facilitates the implementation of ISAC systems for low-altitude aerial vehicles.

C. ISAC Framework

The ISAC framework is shown in Fig. 2, where an aerial vehicle flying in low-altitude airspace is served by multiple uplink BSs. Within the cooperative ISAC framework, the uplink signal is received by multiple BSs. This multi-BS cooperation is fundamental to the framework, offering dual advantages. For communication, it enables joint decoding to enhance signal quality through spatial diversity. For sensing, it is a core requirement, as the individual Doppler measurements from K distributed uplink BSs must be collected to form the system of equations needed to solve for the target's unique position and velocity. These received signals are affected by the Doppler shift caused by the motion of the aerial vehicle, leading to CFO which can cause signal constellation distortion. Each BS estimates and compensates the CFO using the CP-based method. For the communication module of our ISAC framework, these corrected signals are jointly decoded with the MRC algorithm.

For the sensing module of our ISAC framework, the estimated Doppler shifts naturally provided by the OFDM system serve as the key input. Due to noise interference, the estimated Doppler shift obtained from the CFO estimation may be inaccurate, affecting the estimation of the aerial vehicle's position and velocity. Therefore, a learning-based filter is used to improve the accuracy of Doppler shift estimations by leveraging their temporal correlations. Then, the recovered values are used to build the system of equations about the Doppler shift. By substituting the known BS location $\mathbf{s}^{(b)}$, the carrier frequency f_c, and the speed of light c into the system equations, the unknown position $\mathbf{p}$ and velocity $\mathbf{v}$ of the aerial vehicle at a single time step can be obtained. The estimated positions of the aerial vehicle over multiple time steps are then collected to form a continuous trajectory. Finally, the Kalman filter is used to improve the accuracy of trajectory tracking.

The proposed multiple BSs cooperative ISAC framework eliminates the need for additional transmissions of dedicated sensing signals by fully exploiting the inherent Doppler information embedded in OFDM communication signals. This approach also avoids the complex processing associated with echo signals. Unlike conventional radar-based ISAC systems, which require additional sensing transmissions and incur significant time-frequency resource costs, Doppler-based ISAC systems achieve sensing without additional overhead. Furthermore, conventional echo-based localization methods require computationally intensive signal processing, whereas Doppler-based localization simplifies the process of solving a system of equations. This results in a more efficient and resource-saving approach to joint communication and sensing.

D. Multiple Base Stations Joint Decoding

Multi-BS joint decoding for low-altitude aerial vehicles is a cooperative communication technique in which uplink signals transmitted by the aerial vehicle are simultaneously received and processed by multiple BSs. By combining the signals received at different BSs, the system effectively enhances the signal-to-noise ratio (SNR) and reduces the impact of individual channel impairments. This method leverages the spatial diversity of the received signals to mitigate the effects of channel fading and noise, enhancing communication reliability and signal quality. Furthermore, it enables seamless coverage in challenging environments.

Specifically, the MRC is a signal processing technique used in wireless communication to optimally combine multiple received signals for enhanced decoding performance. In MRC, the signals from different BSs are weighted proportionally to their respective channel gains and added coherently, maximizing the overall SNR at the receiver. By assigning greater weighting to higher-quality signals and suppressing the influence of weaker or noisier ones, MRC achieves an optimal combination of spatially diverse signals. This coherent combination enhances the overall quality of the received signal, ensuring more accurate decoding and improving communication reliability, which is particularly beneficial for the communication module of the ISAC framework.

The received time-domain OFDM signal $\tilde{r}^{(b)}(n)$ at b-th BS is transformed to the frequency-domain OFDM symbol $\tilde{R}^{(b)}(m)$ using a discrete Fourier transform, expressed as,

$$\tilde{R}^{(b)}(m) = \frac{1}{\sqrt{M}} \sum_{n=0}^{M-1} \tilde{r}^{(b)}(n) e^{-j\frac{2\pi mn}{M}}, \quad m = 0, \ldots, M-1. \tag{11}$$

The input-output relationship in the frequency domain is then modeled as,

$$\tilde{R}^{(b)}(m) = H^{(b)}(m)X(m) + W^{(b)}(m), \tag{12}$$

where $H^{(b)}(m)$ represents the channel gain at b-th BS and $W^{(b)}(m)$ denotes the noise in the frequency domain. Equation (12) establishes a direct relationship between the transmitted and received OFDM symbols, explicitly accounting for the channel gain and noise. The channel gain $H^{(b)}(m)$ plays a pivotal role in calculating the weighting coefficient $\omega_m^{(b)}$ for MRC, which is defined as,

$$\omega_m^{(b)} = H^{*(b)}(m). \tag{13}$$

These weighting coefficients determine how signals from multiple BSs are optimally combined, exploiting spatial diversity to enhance signal quality. Then, the final combined frequency-domain OFDM symbol $Y(m)$ is obtained by summing the weighted signals from all K cooperating BSs,

$$Y(m) = \sum_{b=1}^{K} \omega_m^{(b)} \tilde{R}^{(b)}(m). \tag{14}$$

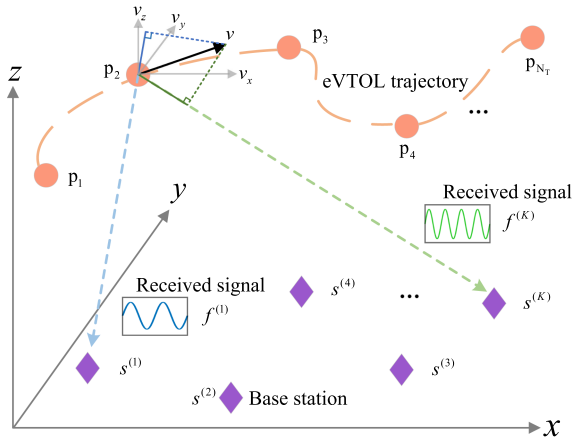

Fig. 3. Doppler shift localization for aerial vehicles.

Substitute (12) into (14), and the combined received signal can be expressed as,

$$Y(m) = \left(\sum_{b=1}^{K} |H^{(b)}(m)|^2 \right) X(m) + \sum_{b=1}^{K} H^{*(b)}(m) W^{(b)}(m). \tag{15}$$

This expression shows that MRC amplifies the transmitted signal by a factor proportional to the sum of the channel power gains while preserving the impact of noise. After MRC processing, the signal $Y(m)$ is fed into the demodulation and decoding stages, where the original frequency-domain OFDM symbol $X(m)$ is recovered.

To evaluate the performance of the received signal after MRC processing, the SNR after MRC is calculated by considering the signal power and noise power as,

$$SNR_{\text{MRC}} = \frac{\left| \sum_{b=1}^{K} |H^{(b)}(m)|^2 \right|^2 P_s}{\sum_{b=1}^{K} |H^{(b)}(m)|^2 \sigma^2}, \tag{16}$$

where $P_s = \mathbb{E}[|X(m)|^2]$ is the signal power and σ^2 is the noise power. Simplifying further, the SNR can be expressed as,

$$SNR_{\text{MRC}} = \frac{P_s}{\sigma^2} \sum_{b=1}^{K} |H^{(b)}(m)|^2. \tag{17}$$

This joint processing ensures robust communication by utilizing the spatial diversity provided by multiple BSs, compensating for channel impairments, and enhancing signal quality.

IV. Localization Using Doppler Shift

In this section, we first present how Doppler shift can be used for target localization. Then, we formulate the Doppler shift based localization problem in the presence of noise as an optimization task. Finally, we introduce our localization algorithm under noisy conditions within a single time step.

A. Doppler Shift for Localization

A simplified model for the 3D localization of the sensing module in our ISAC framework is shown in Fig. 3. The localization task involves estimating the target's position and velocity at a given time instant. The aerial vehicle is assumed to be located at

an unknown position $\mathbf{p} = [p_x, p_y, p_z]^\top \in \mathbb{R}^3$ and moving with an unknown velocity $\mathbf{v} = [v_x, v_y, v_z]^\top \in \mathbb{R}^3$. The aerial vehicle transmits OFDM signals at a known carrier frequency f_c and this signal is received by K spatially distributed BSs, each positioned at known coordinates $\mathbf{s}^{(b)} = [s_x^{(b)}, s_y^{(b)}, s_z^{(b)}]^\top \in \mathbb{R}^3$. The duration of the OFDM signal is very short, so the position and speed of the aerial vehicle can be considered constant during this period. Each BS naturally provides the Doppler shift information of the received signal from the CFO compensation process. This Doppler estimation process is seamlessly integrated into the ISAC framework, leveraging inherent communication signals without requiring additional resource consumption.

We begin by assuming noiseless Doppler shift measurements and focus on the single-point case. The Doppler shift of the received signal is determined by the radial velocity component, which represents the projection of the aerial vehicle's velocity onto the line connecting the aerial vehicle and the BS. The radial velocity, responsible for the observed Doppler shift, depends on the relative position and velocity of the vehicle with respect to the b-th BS. Then, the Doppler shift measured by the b-th BS can then be expressed as,

$$f^{(b)} = \frac{f_c(\mathbf{p} - \mathbf{s}^{(b)})^\top \mathbf{v}}{c\|\mathbf{p} - \mathbf{s}^{(b)}\|}, \tag{18}$$

where $\|\cdot\|$ denotes the Euclidean vector norm, $\frac{(\mathbf{p}-\mathbf{s}^{(b)})}{\|\mathbf{p}-\mathbf{s}^{(b)}\|}$ is the unit vector pointing from the b-th BS to the aerial vehicle, f_c is the known carrier frequency, and c is the known speed of light. To simplify the geometric formulation and eliminate dependencies on the carrier frequency, we define $\delta^{(b)} \triangleq cf^{(b)}/f_c$, which represents the Doppler-derived radial velocity of the aerial vehicle relative to the b-th BS. The expression for this Doppler-derived radial velocity measurement can thus be written as,

$$\delta^{(b)} = \frac{(\mathbf{p} - \mathbf{s}^{(b)})^\top \mathbf{v}}{\|\mathbf{p} - \mathbf{s}^{(b)}\|}, \tag{19}$$

where $\delta^{(b)}$ provides a representation of the Doppler shift, directly related to the relative position and velocity of the aerial vehicle with respect to the b-th BS. This approach is adaptive to any carrier frequency. By means of the Doppler formulation, we establish equations that include the position and velocity of the vehicle as unknown variables.

B. Localization Problem Formulation

The localization process begins by utilizing Doppler shift measurements from multiple BSs, with each BS contributing an independent Doppler shift equation. By combining these measurements, a system of equations is constructed to solve for the unknown position and velocity of the aerial vehicle. In the noiseless scenario, the position $\mathbf{p}$ and velocity $\mathbf{v}$ can be determined by solving the following system of equations,

$$\delta^{(b)}\|\mathbf{p} - \mathbf{s}^{(b)}\| - (\mathbf{p} - \mathbf{s}^{(b)})^\top \mathbf{v} = 0, \quad \text{for } b = 1, \ldots, K, \tag{20}$$

where $b = 1, \ldots, K$ indexes the total K BSs. Each equation encapsulates the relationship between the normalized Doppler shift $\delta^{(b)}$, the relative geometry of the vehicle and the b-th BS, and the vehicle's velocity. When $K \geq 7$, the system usually admits a unique solution for the vehicle's position $\mathbf{p}$ and velocity $\mathbf{v}$ [32]. This condition ensures that the localization problem is well-posed and solvable in typical scenarios.

Next, we consider the scenario where Doppler shift estimations are corrupted by noise. In this case, the inaccurate Doppler shift observed at the b-th BS $\hat{f}^{(b)}$ is expressed as,

$$\hat{f}^{(b)} = f^{(b)} + \eta^{(b)} = \frac{f_c(\mathbf{p} - \mathbf{s}^{(b)})^\top \mathbf{v}}{c\|\mathbf{p} - \mathbf{s}^{(b)}\|} + \eta^{(b)}, \tag{21}$$

where $\eta^{(b)}$ represents the estimation errors introduced during the measurement process. Following the same normalization applied in the noiseless case, we define the normalized noisy Doppler shift as $\hat{\delta}^{(b)} \triangleq c\hat{f}^{(b)}/f_c$. In the presence of noise, the original system of equations in (20) no longer has an exact solution for the target's position and velocity. Specifically, by replacing the ideal, noiseless value $\delta^{(b)}$ from (20) with the noisy measurement $\hat{\delta}^{(b)}$, the term $\delta^{(b)}\|\mathbf{p} - \mathbf{s}^{(b)}\| - (\mathbf{p} - \mathbf{s}^{(b)})^\top \mathbf{v}$ will no longer be equal to zero. To determine the optimal state $\mathbf{x} = [\mathbf{p}^\top, \mathbf{v}^\top]^\top$, we define the residual for the b-th BS as,

$$F_b(\mathbf{x}) = \hat{\delta}^{(b)}\|\mathbf{p} - \mathbf{s}^{(b)}\| - (\mathbf{p} - \mathbf{s}^{(b)})^\top \mathbf{v}. \tag{22}$$

By stacking these residuals, the localization problem is formulated as a nonlinear least squares task,

$$\hat{\mathbf{x}} = \arg\min_{\mathbf{x}} S(\mathbf{x}) = \frac{1}{2}\|\mathbf{F}(\mathbf{x})\|_2^2, \tag{23}$$

where $\mathbf{F}(\mathbf{x}) = [F_1(\mathbf{x}), \ldots, F_K(\mathbf{x})]^\top \in \mathbb{R}^K$ is the residual vector. The Doppler observations at distributed BSs are physically linked because they represent measurements of the same underlying motion state $(\mathbf{p}, \mathbf{v})$. This physical coupling is the fundamental enabler of our localization approach, allowing the unknown state to be resolved by combining observations from multiple spatial perspectives.

C. Localization Algorithm

The nonlinear least-squares optimization approach is a suitable method for addressing the localization problem in this study. Its primary objective is to minimize the target function, thereby determining the optimal parameter vector. This approach efficiently handles scenarios with noisy Doppler shift measurements by leveraging gradient-based techniques to ensure convergence toward the optimal solution.

The Levenberg-Marquardt (LM) algorithm is employed to solve the localization problem, which combines the strengths of the Gauss-Newton method and gradient descent. The LM algorithm is particularly effective in handling ill-conditioned problems. By adaptively adjusting the step size and direction based on the local curvature of the problem, the LM algorithm achieves robust and efficient convergence.

The core of the LM algorithm is the computation of the residual vector and the Jacobian matrix at the current estimate of the state vector $\mathbf{x} = [\mathbf{p}^\top, \mathbf{v}^\top]^\top$. At the k-th iteration, the residual vector $\mathbf{F}(\mathbf{x})$ evaluated at the current parameter estimate $\mathbf{x}_k$ is defined as,

$$\mathbf{F}(\mathbf{x}_k) = [F_1(\mathbf{x}_k), \ldots, F_K(\mathbf{x}_k)]^\top \in \mathbb{R}^K. \tag{24}$$

The Jacobian matrix $\mathbf{J}_k \in \mathbb{R}^{K\times 6}$ contains the first-order partial derivatives of the residual vector $\mathbf{F}(\mathbf{x})$ with respect to the

Algorithm 1: Doppler shift based localization algorithm.

Require: Residual vector $\mathbf{F}(\mathbf{x})$; Initial guess $\mathbf{x}_0 = (\mathbf{p}_0, \mathbf{v}_0)$; Initial damping parameter $\lambda > 0$; Gain factor $\nu > 1$; Tolerance ϵ; Maximum iterations $k_{\max}$; Initialize counter $k = 0$.

while $k < k_{\max}$ **do**
  Evaluate $F_k = \mathbf{F}(\mathbf{x}_k)$ and Jacobian matrix $\mathbf{J}_k = \frac{\partial F}{\partial \mathbf{x}}|_{\mathbf{x}=\mathbf{x}_k}$
  Form the augmented normal equation matrix $\mathbf{A} = \mathbf{J}_k^\top \mathbf{J}_k + \lambda_k \mathbf{I}$
  Solve the linear system $\mathbf{A}\Delta\mathbf{x}_k = -\mathbf{J}_k^\top F_k$ for $\Delta\mathbf{x}_k$
  Compute the new parameters $\mathbf{x}_{k+1} = \mathbf{x}_k + \Delta\mathbf{x}_k$, new objective function value $S(\mathbf{x}_{k+1}) = \frac{1}{2}\|\mathbf{F}(\mathbf{x}_{k+1})\|_2^2$, current objective function value $S(\mathbf{x}_k) = \frac{1}{2}\|\mathbf{F}(\mathbf{x}_k)\|_2^2$
  if $S(\mathbf{x}_{k+1}) < S(\mathbf{x}_k)$ **then**
    Accept the new parameters $\mathbf{x} \leftarrow \mathbf{x}_{k+1}$
    Decrease the damping parameter $\lambda_{k+1} \leftarrow \lambda_k/\nu$
    $k \leftarrow k + 1$
    if $\|\Delta\mathbf{x}_k\|_2 < \epsilon$ **then**
      break
    end if
  else
    Increase the damping parameter $\lambda_k \leftarrow \lambda_k \times \nu$
  end if
end while
return $\mathbf{x} = (\mathbf{p}, \mathbf{v})$

parameters, which is given as,

$$\mathbf{J}_k = \left.\frac{\partial \mathbf{F}}{\partial \mathbf{x}}\right|_{\mathbf{x}=\mathbf{x}_k}. \tag{25}$$

It provides critical information about the local behavior of the residual function, enabling the algorithm to adapt its updates effectively. The b-th row of $\mathbf{J}_k$ is given by,

$$\mathbf{J}_b = \left[\left(\hat{\delta}^{(b)}\frac{\mathbf{p}-\mathbf{s}^{(b)}}{\|\mathbf{p}-\mathbf{s}^{(b)}\|} - \mathbf{v}\right)^\top, -(\mathbf{p}-\mathbf{s}^{(b)})^\top\right]. \tag{26}$$

To determine the update $\Delta\mathbf{x}_k$, the LM algorithm formulates the augmented normal equation,

$$(\mathbf{J}_k^\top \mathbf{J}_k + \lambda_k \mathbf{I})\Delta\mathbf{x}_k = -\mathbf{J}_k^\top \mathbf{F}(\mathbf{x}_k), \tag{27}$$

where $\mathbf{I}$ is the identity matrix. The damping parameter λ_k balances the step size and direction of the update. A larger λ_k biases the update toward gradient descent, ensuring stability, while a smaller λ_k exploits the Gauss-Newton method for faster convergence near the minimum. Once $\Delta\mathbf{x}_k$ is computed by solving (27), the parameter vector is updated as,

$$\mathbf{x}_{k+1} = \mathbf{x}_k + \Delta\mathbf{x}_k. \tag{28}$$

This updated parameter vector $\mathbf{x}_{k+1}$ is then used to evaluate the objective function at the new estimate, defined as,

$$S(\mathbf{x}_{k+1}) = \frac{1}{2}\|\mathbf{F}(\mathbf{x}_{k+1})\|_2^2, \tag{29}$$

where $S(\mathbf{x}_{k+1})$ is the squared Euclidean norm of the residual function $\mathbf{F}(\mathbf{x}_{k+1})$. Simultaneously, the current objective function value, before applying the update, is noted as,

$$S(\mathbf{x}_k) = \frac{1}{2}\|\mathbf{F}(\mathbf{x}_k)\|_2^2. \tag{30}$$

The comparison between $S(\mathbf{x}_{k+1})$ and $S(\mathbf{x}_k)$ determines whether the update is accepted. If $S(\mathbf{x}_{k+1}) < S(\mathbf{x}_k)$, the update is successful, and the damping parameter λ_k is decreased, allowing for larger steps in subsequent iterations. Conversely, if $S(\mathbf{x}_{k+1})$ does not decrease, the update is rejected, and λ_k is increased to enforce smaller, more conservative steps.

As outlined in Algorithm 1, the iterative process continues, dynamically adjusting the damping parameter and updating the parameter vector until one of the convergence criteria is satisfied. By iteratively refining the parameter vector and adaptively adjusting the damping parameter, the algorithm achieves an optimal balance between convergence speed and stability. It provides a powerful and flexible approach to solving localization problems, enabling effective and accurate localization in challenging scenarios.

V. Trajectory Tracking

While Section IV provided the method for localizing the aerial vehicle at a single time slot, practical applications require continuous trajectory tracking. In this section, we begin with the definition and characteristics of time-continuous localization. Then, we present the learning-based filters to improve the Doppler shift estimation accuracy. Finally, we describe the application of the Kalman filter which facilitates effective trajectory tracking.

A. Time-Continuous Localization

Trajectory tracking requires time-continuous localization, and its accuracy can be significantly improved by exploiting the temporal correlation of Doppler shifts and position due to the continuous and predictable nature of aerial vehicle motion. Temporal correlation exists because the position and velocity of a moving target, such as an aerial vehicle, evolve smoothly over time, governed by fundamental kinematic principles. This smooth evolution leads to gradual changes in the observed Doppler shifts, as they are directly related to the relative velocity between the target and BSs. By leveraging this temporal consistency, deep learning models and filtering techniques, such as LSTM networks and Kalman filters, can utilize past and present Doppler measurements and estimated positions to refine the target's current state. This correlation provides a robust foundation for distinguishing true motion patterns from random fluctuations, especially valuable in mitigating the effects of noise and measurement errors. Consequently, incorporating temporal correlation into trajectory tracking algorithms can enhance the accuracy and reliability of localization in dynamic, noisy environments.

To enhance the trajectory tracking accuracy of low-altitude aerial vehicles, we propose a learning-based adaptive double-filter (LADF) localization algorithm, as shown in Fig. 4. The LADF algorithm combines a long short-term memory (LSTM)

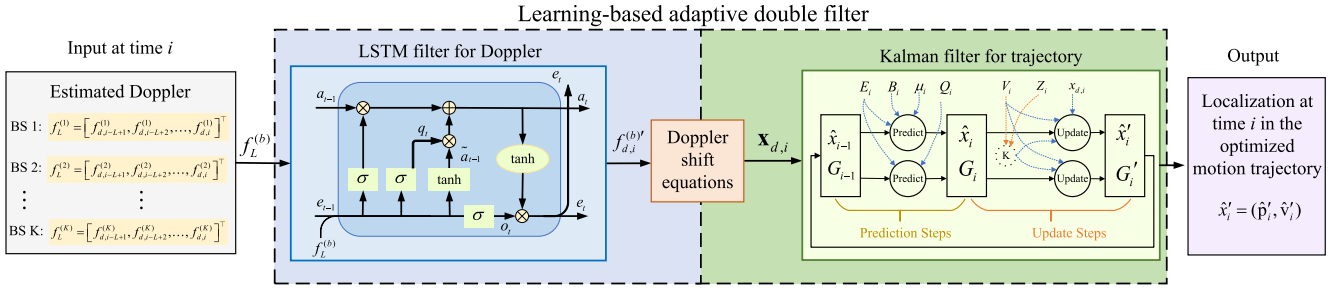

Fig. 4. Learning-based adaptive double filter (LADF) localization algorithm for trajectory tracking.

filter for Doppler shift refinement with a Kalman filter for trajectory optimization. At time i, the Doppler shift measurement at the b-th BS is denoted as $f_{d,i}^{(b)}$. Over L consecutive time steps, the Doppler shift values collected from the b-th BS are aggregated into a set $f_L^{(b)}$, which serves as the input to the LSTM filter. The LSTM filter leverages its ability to model temporal dependencies and smooths out noise-induced errors, providing an optimized Doppler shift estimate $f_L^{(b)'}$. These refined Doppler values are then used in the Doppler shift equations to obtain localization data at time i. The resulting localization data are treated as the measurement observation $\mathbf{x}_{d,i}$ of the Kalman filter, which then performs state estimation to further refine the vehicle trajectory. The Kalman filter applies predictive and corrective steps to further refine the localization data, ultimately producing the aerial vehicle's real-time optimized position as the output of the LADF algorithm. This integration of the LSTM and Kalman filters ensures robust and accurate trajectory tracking, even under noisy measurement conditions.

B. Doppler Shift Estimation With Learning-Based Filter

In the noisy scenario, the Doppler shifts measured by BS over a period can be regarded as a noise-corrupted time series. To enhance the accuracy of localization, we utilize LSTM to process and smooth the Doppler shift sequence, reducing noise in the estimation. For the b-th BS at time i, we take $f_L^{(b)} = [f_{d,i-L+1}^{(b)}, f_{d,i-L+2}^{(b)}, \ldots, f_{d,i}^{(b)}]^\top \in \mathbb{R}^L$ as an input of length L of the LSTM, and aim to output the denoised Doppler shift at the current moment.

The LSTM network is composed of several key components: the input gate, forget gate, output gate, and cell state. These components collaboratively regulate the flow of information, enabling the network to retain relevant information across sequences while discarding irrelevant or noisy information. The forget gate controls how much of the previous cell state should be discarded, which is operated as,

$$g_t = \sigma(D_g f_{L,t}^{(b)} + U_g e_{t-1} + l_g), \quad t = 1, 2, \ldots, L, \tag{31}$$

where $f_{L,t}^{(b)}$ is the t-th element of the input sequence $f_L^{(b)}$, $\sigma(\cdot)$ is the sigmoid activation function, D_g and U_g are weight matrices, e_{t-1} is the hidden state, and l_g is the bias vector for the forget gate. The input gate controls how much new information from the input $f_{L,t}^{(b)}$ influences the cell state, which is operated as,

$$q_t = \sigma(D_q f_{L,t}^{(b)} + U_q e_{t-1} + l_q), \tag{32}$$

where D_q, U_q, and l_q represent the weight matrices and bias vectors for the input gate. To add new information to the cell state, the candidate cell state $\tilde{a}_t$ is calculated as,

$$\tilde{a}_t = \tanh(D_a f_{L,t}^{(b)} + U_a e_{t-1} + l_a), \tag{33}$$

where $\tanh(\cdot)$ is the hyperbolic tangent activation function, D_a, U_a, and l_a are the weight matrices and bias vector for the candidate cell state. By combining the previous cell state a_{t-1} and the candidate cell state $\tilde{a}_t$, the cell state a_t is updated as,

$$a_t = g_t \circ a_{t-1} + q_t \circ \tilde{a}_t, \tag{34}$$

where $\circ$ denotes element-wise multiplication, allowing each component of a_t to be individually regulated. The output gate determines the extent to which the cell state a_t contributes to the hidden state e_t, which is operated as,

$$o_t = \sigma(D_o f_{L,t}^{(b)} + U_o e_{t-1} + l_o), \tag{35}$$

where D_o, U_o, and l_o are the weight matrices and bias vectors for the output gate. The hidden state e_t is then updated by applying the output gate o_t to the hyperbolic tangent of the updated cell state a_t as,

$$e_t = o_t \circ \tanh(a_t). \tag{36}$$

This e_t serves as the output of the LSTM unit at t-th recurrent step, which can be used for subsequent computations or predictions. Finally, the corrected Doppler shift $f_{d,i}^{(b)'}$ is obtained by the last hidden state e_L passed through a linear layer as,

$$f_{d,i}^{(b)'} = D_j e_L + l_j, \tag{37}$$

where D_j and l_j are the weights and bias of the linear layer.

Utilizing the LSTM network for smoothing noisy Doppler shift sequences offers significant advantages within the ISAC framework for aerial vehicle trajectory tracking. The gated architecture of the LSTM network is highly effective at capturing complex temporal dependencies inherent in Doppler shift data, enabling adaptive filtering tailored to dynamic and noisy environments. By employing an LSTM-based filter, noise in the Doppler shift measurements can be effectively mitigated while preserving essential signal features, resulting in enhanced localization accuracy and improved trajectory tracking performance.

C. Position Estimation With Kalman Filter

We employ the Kalman filter to improve the accuracy of trajectory tracking, which uses the observation value from the previous time step combined with an internally constructed mathematical model to calculate a predicted value. The input to the Kalman filter consists of the time-continuous positions obtained by solving the system of equations derived from Doppler shift measurements. The primary objective of the Kalman filter in this framework is to mitigate the impact of noise inherent in the measurement process and to provide accurate, real-time localization of the aerial vehicle. By recursively integrating past and current position estimates with the system dynamics, the Kalman filter ensures smooth and accurate trajectory tracking, even under noisy and dynamic operating conditions.

The operation of the Kalman filter involves two main phases: the prediction and update steps. In the prediction phase, the predicted state vector at time i is calculated as,

$$\hat{\mathbf{x}}_i = \mathbf{E}\hat{\mathbf{x}}_{i-1} + \mathbf{B}\mathbf{u}_i, \tag{38}$$

where $\mathbf{E}$ is the state transition matrix that models the dynamics of the system, $\mathbf{B}$ is the control input matrix, and $\mathbf{u}_i$ is the control input vector at time i. The predicted covariance matrix, which represents the uncertainty of the predicted state, is computed as,

$$\mathbf{G}_i = \mathbf{E}\mathbf{G}_{i-1}\mathbf{E}^\top + \mathbf{Q}, \tag{39}$$

where $\mathbf{G}_{i-1}$ is the covariance matrix from the previous time step, $\mathbf{Q}$ is the process noise covariance that accounts for uncertainties in the system model, and $\mathbf{E}$ propagates the covariance forward in time. The update phase incorporates new measurements to refine the predicted state and covariance. The Kalman gain $\mathbf{O}_i$, which determines the weight given to the measurement in the update process, is calculated as,

$$\mathbf{O}_i = \mathbf{G}_i\mathbf{V}^\top \left(\mathbf{V}\mathbf{G}_i\mathbf{V}^\top + \mathbf{Z}\right)^{-1}, \tag{40}$$

where $\mathbf{V}$ is the observation model matrix that maps the state space to the observation space, and $\mathbf{Z}$ is the measurement noise covariance matrix. After computing $\mathbf{O}_i$, the residual between the position observation $\mathbf{z}_i$ and the predicted value $\mathbf{V}\hat{\mathbf{x}}_i$ is used to update the state estimate as,

$$\hat{\mathbf{x}}'_i = \hat{\mathbf{x}}_i + \mathbf{O}_i(\mathbf{z}_i - \mathbf{V}\hat{\mathbf{x}}_i), \tag{41}$$

where $\mathbf{z}_i \in \mathbb{R}^3$ is the observed position vector derived from the solver at time step i.

Simultaneously, the covariance matrix is updated to reflect the reduced uncertainty after incorporating the new measurement,

$$\mathbf{G}'_i = \mathbf{G}_i - \mathbf{O}_i\mathbf{V}\mathbf{G}_i, \tag{42}$$

where $\mathbf{G}'_i$ is the updated covariance matrix used for the next time step. We adopt a standard constant velocity motion model, which is a common and effective assumption for tracking problems over short time intervals Δt. Based on this, the state transition matrix $\mathbf{E}$ is defined as,

$$\mathbf{E} = \begin{pmatrix} \mathbf{I}_3 & \Delta t \cdot \mathbf{I}_3 \\ \mathbf{0}_3 & \mathbf{I}_3 \end{pmatrix}, \tag{43}$$

where the time interval $\Delta t = N_{sym}(M + N_C)T_s$ is consistent with the Doppler estimation window, with N_{sym} being the number of OFDM symbols used for each Doppler shift estimation. The control input matrix $\mathbf{B}$ is set to zero, and the observation model matrix $\mathbf{V} = [\mathbf{I}_3, \mathbf{0}_3]$ extracts the position components from the state vector to align with the measurements $\mathbf{z}_i$.

By recursively integrating past and current position estimates with system dynamics, the Kalman filter ensures robust and accurate real-time trajectory tracking for aerial vehicles, even in the presence of noise and dynamic operating conditions. As a critical component and the final output module, the Kalman filter works synergistically with the LSTM filter within the LADF algorithm. This integration leverages the predictive capabilities of the Kalman filter and the noise-mitigation strengths of the LSTM filter, forming a solid foundation for achieving accurate and reliable trajectory tracking essential for eVTOL operations.

VI. Simulation Results

In this section, the simulation setup of the low-altitude ISAC system is first given. Then, we present the communication performance based on multiple BSs using MRC. Finally, the time-discrete and time-continuous localization performance are presented respectively.

A. Simulation Setup

We consider a network comprising 10 uplink BSs for cooperative passive ISAC designed to support low-altitude aerial vehicle operations. The path loss between aerial vehicle and the BS is $20log_{10}(f_c) + 20log_{10}(d) + 32.44$ dB, where f_c is carrier frequency in MHz, d is the distance in kilometers. The LSTM network used in the framework has a hidden state size of 64 and consists of 2 layers. For the Kalman filter, the noise covariance matrices are set as $\mathbf{Q} = 0.1\mathbf{I}_6$ and $\mathbf{Z} = 10\mathbf{I}_3$ to match the dimensions of the state vector and position measurements, respectively. An empirical noise-matrix setting balances trust between the model and measurements, where $\mathbf{Z} \gg \mathbf{Q}$ makes the filter rely more on prediction. Additional simulation parameters are provided in Table II [102], [103].

B. Communication Performance

To evaluate the communication performance of the cooperative ISAC framework, we show the SNR after MRC in Fig. 5. It is important to note that this communication analysis is independent of the sensing requirements, and our goal here is to demonstrate the fundamental gains of MRC spatial diversity, which scales with any number of BSs. The simulation considers K BSs with the best channel quality as the service set, where K varies from 1 to 10. The aerial vehicle hovers at altitudes of 200 m, 400 m, and 600 m. It can be seen that as the number of serving BSs increases, the SNR of the received signal also increases accordingly, proving that the scheme of joint decoding with MRC is effective. Meanwhile, the lower the height of the aerial vehicle, the closer the distance to the BSs, and the SNR will increase accordingly. As shown in Fig. 5(f), the results demonstrate that increasing the number of BSs significantly enhances SNR due to spatial diversity, as signals from multiple BSs are coherently combined to mitigate the effects of path loss. Notably, even at higher altitudes, where individual signal quality diminishes due to increased path loss, the cooperation

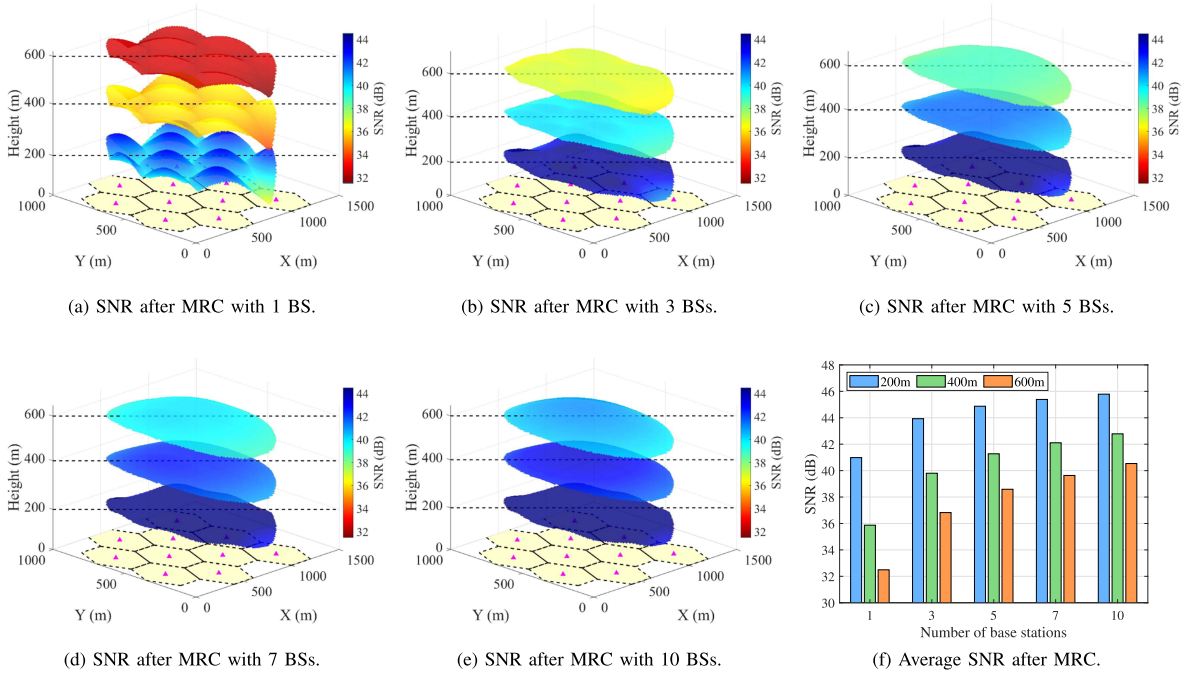

(a) SNR after MRC with 1 BS. (b) SNR after MRC with 3 BSs. (c) SNR after MRC with 5 BSs.

(d) SNR after MRC with 7 BSs. (e) SNR after MRC with 10 BSs. (f) Average SNR after MRC.

Fig. 5. SNR after MRC with different number of BSs.

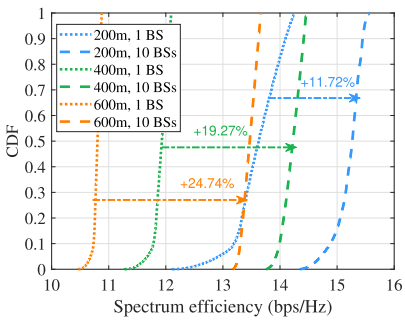

Fig. 6. CDF of spectral efficiency after MRC with different number of BSs.

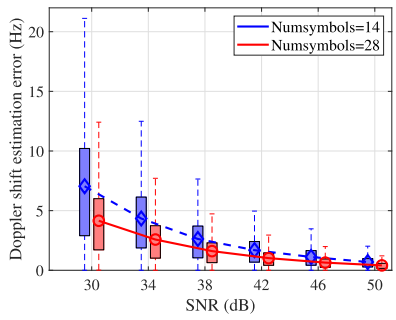

Fig. 7. Estimation error with different symbols.

of more BSs offsets these limitations by enhancing diversity gain and boosting overall SNR. Furthermore, this cooperative approach reduces the reliance on any single BS, enhancing network resilience and maintaining consistent performance despite potential interruptions or fluctuations in channel conditions.

Fig. 6 shows the cumulative distribution function (CDF) of spectral efficiency after MRC with different number of BSs. The spectral efficiency shown in Fig. 6, measured in bps/Hz, is calculated from the post SNR using the Shannon capacity formula. By comparing the results of using only 1 BS and 10 BSs at different heights respectively, it can be seen that compared with using only 1 BS, the joint decoding of 10 BSs has greatly improved the spectral efficiency of signal transmission. Specifically, for the aerial vehicle flying at 200 m, the average spectral efficiency of using 10 BSs for joint decoding compared to using 1 BS for decoding has increased from 13.5 bps/Hz to 15.0 bps/Hz, with an improvement rate of 11.72 %. When the aerial vehicle is at 400 m, the average spectral efficiency increases from 11.9 bps/Hz to 14.1 bps/Hz, with an increase rate of 19.27 %. Meanwhile, when the aerial vehicle is at 600 m, the average spectral efficiency increases from 10.8 bps/Hz to 13.4 bps/Hz, with an increase rate of 24.74 %. It can be seen from the improvement results that the joint decoding of MRC is effective in enhancing the spectral efficiency in low-altitude environments. Especially at higher altitudes (such as 600 m) and farther from the BSs, the spectral efficiency is relatively low, and the improvement of the joint decoding of MRC is even more significant.

C. Time-Discrete Localization Performance

Fig. 7 shows the Doppler shift estimation error as a function of SNR, averaged from two different numbers of OFDM symbols, including 14 and 28. The results show that estimation error decreases with increasing SNR, indicating improved Doppler shift estimation accuracy at higher SNR levels. Using 28 symbols consistently achieves lower estimation errors compared to 14 symbols, as the additional symbols enable more observations, effectively mitigating noise and enhancing accuracy. Moreover, error variability decreases with higher SNR

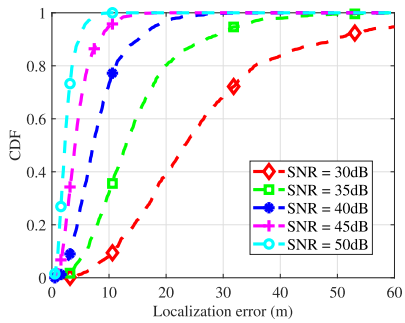

Fig. 8. CDF of time-discrete localization errors.

and is consistently lower for 28 symbols, reflecting enhanced stability and robustness. The CP-based approach efficiently provides reliable Doppler shift measurements without requiring additional pilot signals, making it both resource-efficient and effective. This accurate Doppler shift estimation approach is critical for the sensing module in ISAC systems, ensuring accurate localization. The results further validate the feasibility of Doppler shift-based localization, as the observed low estimation errors, even at moderate SNR levels, highlight its robustness and potential for practical applications in ISAC systems. For the following experiments, we adopt 28 symbols for Doppler shift estimation, and the flying altitude of the aerial vehicle is set to 200 m.

Assuming a constant and consistent SNR across all BSs, Fig. 8 shows the CDF of time-discrete localization errors for discrete-time localization based on Doppler shifts estimated from BSs at different SNR levels. The results highlight the effectiveness of Doppler shift-based localization in ISAC systems, particularly at higher SNR levels, where the accuracy of Doppler shift estimation improves significantly, resulting in accurate localization. For instance, at high SNR levels, the majority of localization errors are small, showcasing the high precision achievable with reliable Doppler shift measurements. Even at moderate SNR levels, Doppler-based localization demonstrates robustness, with errors remaining within acceptable ranges for practical applications. This analysis underscores the effectiveness of Doppler shift-based localization as the sensing module in the ISAC system, enabling accurate and reliable localization for low-altitude aerial vehicles.

D. Time-Continuous Localization Performance

For time-continuous localization, the accuracy improvement in Doppler shift estimation achieved by leveraging temporal correlation is shown in Fig. 9, where the transmit power of aerial vehicle is 20 dBm. Fig. 9(a) compares the Doppler shift estimation errors for different filters, including historical average (HA), recurrent neural network (RNN), gated recurrent unit (GRU), and LSTM. The HA is a sliding average filter with a window of 5 time steps, and the parameter settings for RNN and GRU are consistent with the LSTM. Among these methods, LSTM demonstrates the best performance in optimizing Doppler shift estimation, reducing the estimation error from approximately 2 Hz to around 0.5 Hz. Fig. 9(b) visualizes the Doppler shift estimation for three BSs, comparing the original estimated Doppler values with those optimized using the LSTM filter. The results show that the LSTM filter produces noticeably smoother Doppler curves, effectively reducing estimation errors by capturing and utilizing the temporal correlations in the Doppler data. This improved accuracy ensures more accurate inputs for subsequent localization algorithms, making the LSTM filter particularly valuable for time-continuous localization. By mining the temporal dependencies inherent in Doppler shifts, the LSTM filter provides a robust and accurate foundation for reliable localization in the ISAC system. The LSTM-filtered Doppler curves exhibit high smoothness, which reflects the filter's ability to capture the inherent physical continuity of the eVTOL's trajectory and ensures more reliable convergence and significantly reduces the occurrence of localization outliers.

Fig. 10 shows the comparison of trajectory tracking results for a low-altitude aerial vehicle flying in a circular path at 200 m with a transmit signal power of 20 dBm. Specifically, Fig. 10(a) shows the results using the original Doppler shift estimation and a Kalman filter, where significant deviations from the true trajectory (dashed green line) are observed in the estimated trajectory before filtering (red points). The filtered trajectory (blue line) shows improvement but still exhibits noticeable errors compared to the true trajectory. In contrast, Fig. 10(b) shows the results using the proposed LADF algorithm, which significantly reduces localization errors and obtains an estimated trajectory that closely aligns with the true trajectory. By leveraging the LSTM filter to refine Doppler shift estimation and the Kalman filter to optimize the trajectory, the LADF algorithm effectively mitigates noise and errors, achieving higher accuracy in trajectory tracking. These results validate the effectiveness of the LADF algorithm in improving time-continuous localization accuracy for aerial vehicles in low-altitude environments. Fig. 10(c) shows the average trajectory tracking error comparison of this circular path with different transmit power. The comparison includes four approaches: the original time-discrete method, the Kalman filter for trajectory, the LSTM filter for Doppler shift, and the proposed LADF algorithm. The results highlight the significant error reduction achieved by the LADF algorithm across all transmit power levels. The integration of LSTM for refining Doppler shift estimation and the Kalman filter for trajectory optimization in the LADF algorithm provides a clear advantage, effectively mitigating noise and leveraging temporal correlations.

When the flight trajectory of the aerial vehicle is a straight line, the visualization of comparisons of trajectory tracking results and average time-continuous localization errors for different transmitter powers are shown in Fig. 11. The results indicate that LADF can significantly improve localization accuracy, reducing errors consistently across different power levels and trajectory types, including circular and straight-line paths. These results validate the LADF algorithm as an effective and robust trajectory tracking approach, especially suited for multiple BSs cooperative ISAC systems tailored for low-altitude aerial vehicles in dynamic and noisy environments.

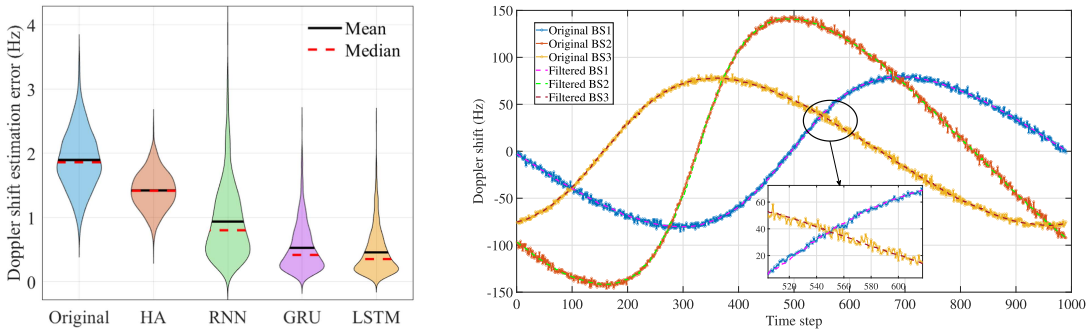

(a) Doppler shift estimation errors of different filters.

(b) Visualization of Doppler shift estimation after LSTM filter.

Fig. 9. Accuracy improvement in Doppler shift estimation by exploiting temporal correlation with filters.

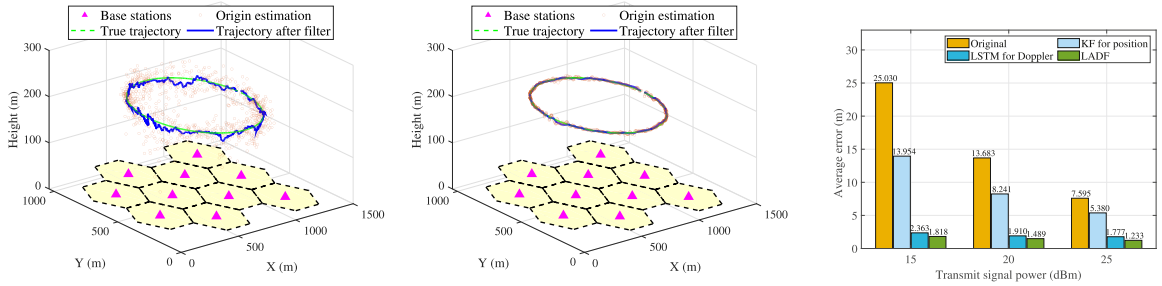

(a) Results using original Doppler shift and KF.

(b) Results using the proposed LADF algorithm.

(c) Trajectory tracking error comparison.

Fig. 10. Trajectory tracking results of a low-altitude aerial vehicle flying in a circle.

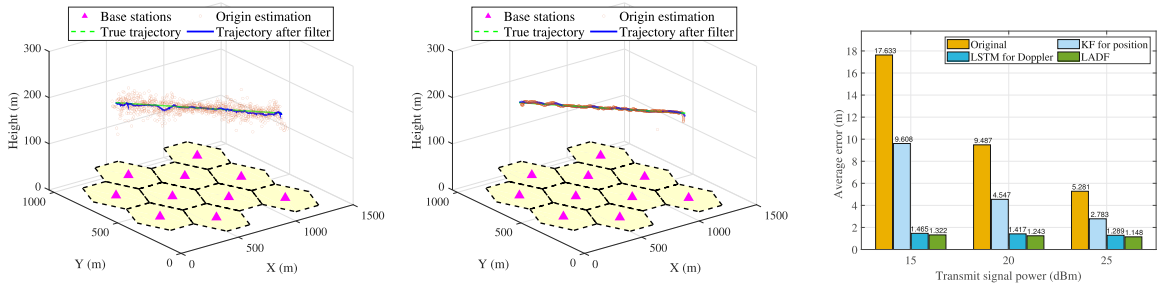

(a) Results using original Doppler shift and KF.

(b) Results using the proposed LADF algorithm.

(c) Trajectory tracking error comparison.

Fig. 11. Trajectory tracking results of a low-altitude aerial vehicle flying in a straight line.

VII. Conclusion

In this paper, we have proposed a multiple BSs cooperative passive ISAC framework for low-altitude aerial vehicles, which leverages existing communication signals without requiring additional time-frequency resource overhead. Additionally, we have proposed a time-continuous localization algorithm named LADF, which utilizes the Doppler shift information inherently provided by the uplink OFDM system. Extensive simulations have demonstrated the effectiveness of the proposed Doppler shift based multiple BSs cooperative ISAC approach for aerial vehicles. The proposed framework provides a cost-effective and spectrum-efficient sensing solution that is well aligned with the requirements of the emerging low-altitude economy. Its passive localization capability can directly support practical applications such as automated drone delivery, urban air mobility traffic management, and collision avoidance in congested airspace. Future work will focus on further improving localization accuracy by integrating Doppler information with additional sensing modalities, such as angle-of-arrival measurements.

References

[1] X. Duan, X. Zhang, S. Xia, Z. Wang, Y. Ma, and W. Yuan, "Machine learning empowered UAV-based beamforming design in ISAC systems," *Sci. China Inf. Sci.*, vol. 68, no. 5, pp. 1–2, 2025.

[2] J. Wu, W. Yuan, Q. Cheng, and H. Jin, "Toward dual-functional LAWN: Control-aware system design for aerodynamics-aided UAV formations," *IEEE J. Sel. Areas Commun.*, vol. 44, pp. 791–804, 2026.

[3] H. Huang, J. Su, and F.-Y. Wang, "The potential of low-altitude airspace: The future of urban air transportation," *IEEE Trans. Intell. Veh.*, vol. 9, no. 8, pp. 5250–5254, Aug. 2024.

[4] G. Sun et al., "Age of information optimization in laser-charged UAVs-assisted IoT networks: A multi-agent deep reinforcement learning method," *IEEE Trans. Netw. Sci. Eng.*, vol. 13, pp. 1436–1457, 2026.

[5] P. Chen et al., "Frisbee: An efficient data sharing framework for UAV swarms," *IEEE Trans. Netw. Sci. Eng.*, vol. 11, no. 6, pp. 5380–5393, Nov./Dec. 2024.

[6] L. Qian, Y. L. Lo, and H. H.-t. Liu, "A path planning algorithm for a crop monitoring fixed-wing unmanned aerial system," *Sci. China Inf. Sci.*, vol. 67, no. 8, 2024, Art. no. 180201.
[7] X. Zheng et al., "UAV swarm-enabled collaborative post-disaster communications in low altitude economy via a two-stage optimization approach," *IEEE Trans. Mobile Comput.*, vol. 24, no. 11, pp. 11833–11851, Nov. 2025.
[8] S. Zhang, S. Zhang, W. Yuan, J. Shi, Z. Li, and T. Q. Quek, "Personalizing rate-splitting in vehicular communication via large multi-modal model," *Sci. China Inf. Sci.*, vol. 68, no. 7, pp. 1–16, 2025.
[9] W. Yuan et al., "Wireless localization and formation control with asynchronous agents," *IEEE J. Sel. Areas Commun.*, vol. 42, no. 10, pp. 2890–2904, Oct. 2024.
[10] Y. Zhang, J. Wang, G. Du, J. Chen, J. Wang, and Q. Li, "ISAC-Aided UAV swarms: From networked perception to capability evolution," *IEEE Commun. Mag.*, vol. 62, no. 9, pp. 60–66, Sep. 2024.
[11] X. Shi, X. Xuan, X. Huang, J. Xue, and X. Shen, "Digital twin empowered wireless positioning: Prospects, architecture, and challenges," *IEEE Netw.*, early access, Feb. 24, 2025, doi: 10.1109/MNET.2025.3544694.
[12] Y. Xu et al., "Fully-Decoupled RAN for feedback-free multi-base station transmission in MIMO-OFDM system," *IEEE J. Sel. Areas Commun.*, vol. 43, no. 3, pp. 780–794, Mar. 2025.
[13] T. Zhang et al., "Toward handover-free mobility management in FD-RAN: Architecture, challenges, and solutions," *IEEE Netw.*, vol. 38, no. 6, pp. 433–442, Nov. 2024.
[14] F. Liu et al., "Integrated sensing and communications: Toward dual-functional wireless networks for 6G and beyond," *IEEE J. Sel. Areas Commun.*, vol. 40, no. 6, pp. 1728–1767, Jun. 2022.
[15] J. Zhang et al., "Intelligent integrated sensing and communication: A survey," *Sci. China Inf. Sci.*, vol. 68, no. 3, 2025, Art. no. 131301.
[16] J. Chen, X. Liang, J. Xue, Y. Sun, H. Zhou, and X. Shen, "Evolution of RAN architectures toward 6G: Motivation, development, and enabling technologies," *IEEE Commun. Surveys Tuts.*, vol. 26, no. 3, pp. 1950–1988, third quarter 2024.
[17] D. Wang et al., "Enhanced ISAC framework for moving target assisted by beyond-diagonal RIS: Accurate localization and efficient communication," *IEEE Trans. Netw. Sci. Eng.*, vol. 12, no. 5, pp. 4299–4315, Sep./Oct. 2025.
[18] N. C. Luong et al., "Advanced learning algorithms for integrated sensing and communication (ISAC) systems in 6G and beyond: A comprehensive survey," *IEEE Commun. Surveys Tuts.*, vol. 28, pp. 2572–2611, 2026.
[19] Q. Cui et al., "Overview of AI and communication for 6G network: Fundamentals, challenges, and future research opportunities," *Sci. China Inf. Sci.*, vol. 68, no. 7, 2025, Art. no. 171301.
[20] Z. Wei et al., "Integrated sensing and communication enabled multiple base stations cooperative sensing towards 6G," *IEEE Netw.*, vol. 38, no. 4, pp. 207–215, Jul. 2024.
[21] Y. Li, Z. Wei, H. Liu, and Z. Feng, "Uplink multi-RSU cooperative sensing strategy for integrated sensing and communication system," *IEEE Trans. Cogn. Commun. Netw.*, vol. 11, no. 5, pp. 3112–3127, Oct. 2025.
[22] J. Xue, T. Jiang, H. Huang, Z. Zhang, H. Zhou, and X. Shen, "Enabling data-driven OTFS modulation for 6G hyper reliable high-mobility communications," *IEEE Wireless Commun.*, vol. 32, no. 3, pp. 196–203, Jun. 2025.
[23] J. Wu and P. Fan, "A survey on high mobility wireless communications: Challenges, opportunities and solutions," *IEEE Access*, vol. 4, pp. 450–476, 2016.
[24] J. Xue, K. Yu, T. Zhang, H. Zhou, L. Zhao, and X. Shen, "Cooperative deep reinforcement learning enabled power allocation for packet duplication URLLC in multi-connectivity vehicular networks," *IEEE Trans. Mobile Comput.*, vol. 23, no. 8, pp. 8143–8157, Aug. 2024.
[25] X. Wei, W. Yuan, K. Zhang, and F. Liu, "OTFS-Assisted ISAC system: Delay Doppler channel estimation and SDR-based implementation," *IEEE Trans. Mobile Comput.*, vol. 24, no. 11, pp. 11865–11878, Nov. 2025.
[26] J. Wu, Y. Shi, W. Yuan, Q. Cheng, B. Li, and X. Wei, "SDR-Empowered environment sensing design and experimental validation using OTFS-ISAC signals," *IEEE Trans. Mobile Comput.*, vol. 24, no. 11, pp. 12252–12263, Nov. 2025.
[27] J. Xue, T. Jiang, Z. Ma, Y. Xu, H. Zhou, and X. Shen, "Predictive beamforming for OTFS-enabled URLLC in high-mobility vehicular networks," *IEEE Trans. Cogn. Commun. Netw.*, vol. 12, pp. 2355–2368, 2026.
[28] J. Liu et al., "OFDM-Structure based waveform designs for integrated sensing and communication," *Sci. China Inf. Sci.*, vol. 68, no. 5, 2025, Art. no. 150306.
[29] S. Singh, S. Kumar, S. Majhi, U. Satija, and C. Yuen, "Blind carrier frequency offset estimation techniques for next-generation multicarrier communication systems: Challenges, comparative analysis, and future prospects," *IEEE Commun. Surveys Tuts.*, vol. 27, no. 1, pp. 1–36, Feb. 2025.
[30] Z. Ma, J. Xue, J. Li, Y. Yuan, X. Liu, and H. Zhou, "Leveraging OTFS modulation for high Doppler shift channel in satellite vehicular networks," in *Proc. Int. Conf. Future Commun. Netw.*, 2024, pp. 1–6.
[31] C. Zhao et al., "BUPTCMCC-6G-CMG : A GBSM-based ISAC standard channel model generator," *Sci. China Inf. Sci.*, vol. 68, no. 5, pp. 1–15, 2025.
[32] I. Shames, A. N. Bishop, M. Smith, and B. D. O. Anderson, "Doppler shift target localization," *IEEE Trans. Aerosp. Electron. Syst.*, vol. 49, no. 1, pp. 266–276, Jan. 2013.
[33] M. M. Ahmed, K. C. Ho, and G. Wang, "3-D target localization and motion analysis based on Doppler shifted frequencies," *IEEE Trans. Aerosp. Electron. Syst.*, vol. 58, no. 2, pp. 815–833, Apr. 2022.
[34] X. Ke and K. C. Ho, "Localization by Doppler derivatives and Doppler-shifted frequencies," *IEEE Trans. Signal Process.*, vol. 72, pp. 2890–2904, 2024.
[35] Z. Wei et al., "Integrated sensing and communication enabled cooperative passive sensing using mobile communication system," *IEEE Trans. Mobile Comput.*, vol. 24, no. 9, pp. 7805–7821, Sep. 2025.
[36] Q. Yu et al., "A fully-decoupled RAN architecture for 6G inspired by neurotransmission," *J. Commun. Inf. Netw.*, vol. 4, no. 4, pp. 15–23, 2019.
[37] T. Zhang et al., "Handover-Free multi-connectivity mobility management for downlink FD-RAN: A hierarchical DRL-based approach," *IEEE Trans. Cogn. Commun. Netw.*, vol. 11, no. 2, pp. 1281–1296, Apr. 2025.
[38] P. Shukla, S. Shukla, and A. K. Singh, "Trajectory-prediction techniques for unmanned aerial vehicles (UAVs): A comprehensive survey," *IEEE Commun. Surveys Tuts.*, vol. 27, no. 3, pp. 1867–1910, Jun. 2025.
[39] Y. Zhu, M. Mallick, S. Liang, and J. Yan, "Generalized labeled multi-Bernoulli multi-target tracking with Doppler-only measurements," *Remote Sens.*, vol. 14, no. 13, 2022, Art. no. 3131.
[40] M. Liang, D. Y. Kim, and X. Kai, "Multi-Bernoulli filter for target tracking with multi-static Doppler only measurement," *Signal Process.*, vol. 108, pp. 102–110, 2015.
[41] T. Ngo, B. T. Kelley, and P. Rad, "Deep learning based prediction of Doppler shift for mobile communications," in *Proc. Telecoms Conf.*, 2021, pp. 1–6.
[42] N. Davari and A. P. Aguiar, "Real-time outlier detection applied to a Doppler velocity log sensor based on hybrid autoencoder and recurrent neural network," *IEEE J. Ocean. Eng.*, vol. 46, no. 4, pp. 1288–1301, Oct. 2021.
[43] J. Xue et al., "Sparse mobile crowdsensing for cost-effective traffic state estimation with spatio–temporal transformer graph neural network," *IEEE Internet Things J.*, vol. 11, no. 9, pp. 16227–16242, May 2024.
[44] X. Huang, W. Wu, S. Hu, M. Li, C. Zhou, and X. Shen, "Digital twin based user-centric resource management for multicast short video streaming," *IEEE J. Sel. Topics Signal Process.*, vol. 18, no. 1, pp. 50–65, Jan. 2024.
[45] J. Xue et al., "Large AI model for delay-Doppler domain channel prediction in 6G OTFS-based vehicular networks," *Sci. China Inf. Sci.*, vol. 68, no. 7, pp. 184–198, 2025.
[46] Y. Sun et al., "LOSEC: Local semantic capture empowered large time series model for IoT-enabled data centers," *IEEE Internet Things J.*, vol. 12, no. 10, pp. 13144–13156, May 2025.
[47] F. Liu, W. Yuan, C. Masouros, and J. Yuan, "Radar-assisted predictive beamforming for vehicular links: Communication served by sensing," *IEEE Trans. Wireless Commun.*, vol. 19, no. 11, pp. 7704–7719, Nov. 2020.
[48] Q. Huang, Z. Song, Z. Xiong, G. Xu, N. Zhao, and D. Niyato, "Robust sensing-assisted secure communication via cooperative base stations," *IEEE Trans. Commun.*, vol. 73, no. 11, pp. 10602–10615, Nov. 2025.
[49] K. Meng, C. Masouros, A. P. Petropulu, and L. Hanzo, "Cooperative ISAC networks: Performance analysis, scaling laws and optimization," *IEEE Trans. Wireless Commun.*, vol. 24, no. 2, pp. 877–892, Feb. 2025.
[50] Y. Feng, C. Zhao, H. Luo, F. Gao, F. Liu, and S. Jin, "Networked ISAC based UAV tracking and handover towards low-altitude economy," *IEEE Trans. Wireless Commun.*, vol. 24, no. 9, pp. 7670–7685, Sep. 2025.
[51] G. Liu et al., "Feasibility study of cooperative sensing: Radar cross section, synchronization, cooperative cluster, performance and prototype," *Sci. China Inf. Sci.*, vol. 68, no. 5, pp. 1–19, 2025.
[52] Y. Fan, S. Wu, X. Bi, and G. Li, "Power allocation for cell-free massive MIMO ISAC systems with OTFS signal," *IEEE Internet Things J.*, vol. 12, no. 7, pp. 9314–9331, Apr. 2025.

[53] Y. Li, Z. Wei, Y. Wang, H. Liu, and Z. Feng, "Cooperative sensing in uplink ISAC system: A multi-user waveform optimization approach," *IEEE Trans. Veh. Technol.*, vol. 74, no. 7, pp. 10943–10957, Jul. 2025.

[54] Y. Song et al., "An overview of cellular ISAC for low-altitude UAV: New opportunities and challenges," *IEEE Commun. Mag.*, vol. 63, no. 12, pp. 88–95, Dec. 2025.

[55] G. Cheng, X. Song, Z. Lyu, and J. Xu, "Networked ISAC for low-altitude economy: Coordinated transmit beamforming and UAV trajectory design," *IEEE Trans. Commun.*, vol. 73, no. 8, pp. 5832–5847, Aug. 2025.

[56] Y. Wang et al., "Toward realization of low-altitude economy networks: Core architecture, integrated technologies, and future directions," *IEEE Trans. Cogn. Commun. Netw.*, vol. 11, no. 5, pp. 2788–2820, Oct. 2025.

[57] K. Xiong, Z. Chen, J. Xie, Y. Qin, S. Leng, and C. Yuen, "Digital twin-based SIM communication and flight control for advanced air mobility," *IEEE Trans. Netw. Sci. Eng.*, vol. 13, pp. 728–744, 2026.

[58] K. Xiong, Y. Chen, Z. He, Y. Qin, S. Leng, and C. Yuen, "Network slice-based low-altitude intelligent network for advanced air mobility," *IEEE Trans. Netw. Sci. Eng.*, vol. 13, pp. 1800–1816, 2026.

[59] Z. Liu et al., "Integrated sensing and edge AI: Realizing intelligent perception in 6G," *IEEE Commun. Surveys Tuts.*, vol. 28, pp. 2725–2770, 2026.

[60] J. Wangjun, W. Zhiqing, F. Zhiyong, and C. Xu, "Integrated sensing and communication enabled sensing base station: System design, beamforming, interference cancellation and performance analysis," *China Commun.*, vol. 22, no. 1, pp. 111–127, Jan. 2025.

[61] Y. Jiang et al., "Integrated sensing and communication for low altitude economy: Opportunities and challenges," *IEEE Commun. Mag.*, vol. 63, no. 12, pp. 72–78, Dec. 2025.

[62] Y. Fang, J. Yang, D. Ma, M. Yang, Z. Xu, and X. Chen, "Integrated sensing and backscatter communication with movable antennas: State-of-the-art survey and a novel inverse scattering framework," *IEEE Trans. Netw. Sci. Eng.*, vol. 13, pp. 4350–4368, 2026.

[63] W. Mao, Y. Lu, C.-Y. Chi, B. Ai, Z. Zhong, and Z. Ding, "Communication-sensing region for cell-free massive MIMO ISAC systems," *IEEE Trans. Wireless Commun.*, vol. 23, no. 9, pp. 12396–12411, Sep. 2024.

[64] X. Shao et al., "Polarforming antenna enhanced sensing and communication: Modeling and optimization," *IEEE J. Sel. Areas Commun.*, vol. 44, pp. 416–431, 2026.

[65] Y. Qiao et al., "Resource allocation for ISAC and HRLLC in UAV-assisted HSR system with a hybrid PSO-genetic algorithm," *IEEE Internet Things J.*, vol. 12, no. 6, pp. 6790–6804, Mar. 2025.

[66] X. Liu et al., "Energy-Minimization resource allocation for FD-NOMA enabled integrated sensing, communication, and computation in PIoT," *IEEE Trans. Netw. Sci. Eng.*, vol. 11, no. 6, pp. 5863–5877, Nov./Dec. 2024.

[67] Z. Zhou, X. Li, G. Zhu, B. Zhou, H. Xing, and K. Huang, "Integrated sensing-communication-computation design for energy efficient data processing," *IEEE Trans. Netw. Sci. Eng.*, vol. 13, pp. 4172–4186, 2026.

[68] J. Wang et al., "Generative AI for integrated sensing and communication: Insights from the physical layer perspective," *IEEE Wireless Commun.*, vol. 31, no. 5, pp. 246–255, Oct. 2024.

[69] J. Wang et al., "Generative AI based secure wireless sensing for ISAC networks," *IEEE Trans. Inf. Forensics Secur.*, vol. 20, pp. 5195–5210, 2025.

[70] J. Wang et al., "Optimizing 6G integrated sensing and communications via expert networks," *IEEE Wireless Commun.*, vol. 32, no. 5, pp. 142–150, Oct. 2025.

[71] X. Xia, Z. Fang, K. Xu, and W. Xie, "An ambiguity-function-assisted active sensing scheme for OFDM-based ISAC systems toward low-altitude airspace," *IEEE Internet Things J.*, vol. 12, no. 12, pp. 19471–19487, Jun. 2025.

[72] J. Wan et al., "Sensing capacity for integrated sensing and communication systems in low-altitude economy," *IEEE Commun. Lett.*, vol. 29, no. 6, pp. 1240–1244, Jun. 2025.

[73] X. Ye, Y. Mao, X. Yu, S. Sun, L. Fu, and J. Xu, "Integrated sensing and communications for low-altitude economy: A deep reinforcement learning approach," *IEEE Trans. Wireless Commun.*, vol. 25, pp. 351–367, 2026.

[74] B. Hu et al., "MADQN-Enhanced computation offloading and resource allocation for 6G low-altitude economy vehicular networks," *IEEE Trans. Cogn. Commun. Netw.*, vol. 12, pp. 2603–2617, 2026.

[75] Z. Wei et al., "Deep cooperation in ISAC system: Resource, node and infrastructure perspectives," *IEEE Internet Things Mag.*, vol. 7, no. 6, pp. 118–125, Nov. 2024.

[76] N. Babu, C. Masouros, C. B. Papadias, and Y. C. Eldar, "Precoding for multi-cell ISAC: From coordinated beamforming to coordinated multipoint and bi-static sensing," *IEEE Trans. Wireless Commun.*, vol. 23, no. 10, pp. 14637–14651, Oct. 2024.

[77] L. Zhou, J. Dai, W. Xu, and C. Chang, "Joint target detection and channel estimation for distributed massive mimo ISAC systems," *IEEE Trans. Cogn. Commun. Netw.*, vol. 11, no. 1, pp. 300–315, Feb. 2025.

[78] Y. Jingxuan et al., "Passive integrated sensing and communication scheme based on RF fingerprint information extraction for cell-free RAN," *China Commun.*, vol. 22, no. 1, pp. 171–181, Jan. 2025.

[79] Z. Zhang et al., "Target localization in cooperative ISAC systems: A scheme based on 5G NR OFDM signals," *IEEE Trans. Commun.*, vol. 73, no. 5, pp. 3562–3578, May 2025.

[80] J. Tang et al., "Cooperative ISAC-empowered low-altitude economy," *IEEE Trans. Wireless Commun.*, vol. 24, no. 5, pp. 3837–3853, May 2025.

[81] F. Li et al., "Cooperative sensing and communication beamforming design for low-altitude economy," *Sci. China Inf. Sci.*, vol. 69, no. 2, 2026, Art. no. 122304.

[82] K. Ji, Q. Zhang, Z. Wei, Z. Feng, and P. Zhang, "Networking based ISAC hardware testbed and performance evaluation," *IEEE Commun. Mag.*, vol. 61, no. 5, pp. 76–82, May 2023.

[83] X. Lu, Z. Wei, R. Xu, L. Wang, B. Lu, and J. Piao, "Integrated sensing and communication enabled multiple base stations cooperative UAV detection," in *Proc. IEEE Int. Conf. Commun. Workshops*, 2024, pp. 1882–1887.

[84] R. Li, Q. Zhang, D. Ma, K. Yu, and Y. Huang, "Joint target assignment and resource allocation for multi-base station cooperative ISAC in UAV detection," *IEEE Trans. Veh. Technol.*, vol. 74, no. 5, pp. 7700–7714, May 2025.

[85] Y. Hu et al., "Collaborative positioning optimization for multiple moving users in UAV-enabled ISAC," *IEEE Trans. Cogn. Commun. Netw.*, vol. 11, no. 5, pp. 3016–3030, Oct. 2025.

[86] K. Meng, K. Han, C. Masouros, and L. Hanzo, "Network-level ISAC: An analytical study of antenna topologies ranging from massive to cell-free MIMO," *IEEE Trans. Wireless Commun.*, vol. 24, no. 12, pp. 10003–10018, Dec. 2025.

[87] M. Elfiatoure, M. Mohammadi, H. Quoc Ngo, H. Shin, and M. Matthaiou, "Multiple-target detection in cell-free massive MIMO-assisted ISAC," *IEEE Trans. Wireless Commun.*, vol. 24, no. 5, pp. 4283–4298, May 2025.

[88] U. Demirhan and A. Alkhateeb, "Cell-Free ISAC MIMO systems: Joint sensing and communication beamforming," *IEEE Trans. Commun.*, vol. 73, no. 6, pp. 4454–4468, Jun. 2025.

[89] X. Sun, W. Xue, J. Li, D. Wang, P. Zhu, and X. You, "Mobility management framework for cooperative cell-free ISAC systems," *IEEE Internet Things J.*, vol. 12, no. 23, pp. 49784–49800, Dec. 2025.

[90] I. S. Mohamad Hashim, A. Al-Hourani, and B. Ristic, "Satellite localization of IoT devices using signal strength and Doppler measurements," *IEEE Wireless Commun. Lett.*, vol. 11, no. 9, pp. 1910–1914, Sep. 2022.

[91] Y.-T. Chan and F. Jardine, "Target localization and tracking from Doppler-shift measurements," *IEEE J. Ocean. Eng.*, vol. 15, no. 3, pp. 251–257, Jul. 1990.

[92] A. Amar and A. J. Weiss, "Localization of narrowband radio emitters based on Doppler frequency shifts," *IEEE Trans. Signal Process.*, vol. 56, no. 11, pp. 5500–5508, Nov. 2008.

[93] T. Jia, K. C. Ho, H. Wang, and X. Shen, "Localization of a moving object with sensors in motion by time delays and Doppler shifts," *IEEE Trans. Signal Process.*, vol. 68, pp. 5824–5841, 2020.

[94] L. Deng, P. Wei, Z. Zhang, and H. Zhang, "Doppler frequency shift based source localization in presence of sensor location errors," *IEEE Access*, vol. 6, pp. 59752–59760, 2018.

[95] J. Wang, Y. Cui, M. Zhou, H. Sun, L. Liu, and A. Zhang, "Doppler shift estimation for downlink OFDM signals in underwater acoustic integrated sensing and communication networks," in *Proc. IEEE Int. Conf. Signal Process.*, 2024, pp. 125–129.

[96] M. M. Ahmed, K. C. Ho, and G. Wang, "Localization of a moving source by frequency measurements," *IEEE Trans. Signal Process.*, vol. 68, pp. 4839–4854, 2020.

[97] Q. Qi, Y. Li, and Q. Guo, "A convex relaxation algorithm for source localization considering sensor motion in wireless sensor networks," *IEEE Commun. Lett.*, vol. 25, no. 6, pp. 1867–1871, Jun. 2021.

[98] X. Meng, Y. Li, Z. Wu, S. Hong, and S. Chang, "A semidefinite relaxation approach for mobile target localization based on TOA and Doppler frequency shift measurements," *IEEE Sensors J.*, vol. 23, no. 14, pp. 16051–16057, Jul. 2023.

[99] M. B. Guldogan, D. Lindgren, F. Gustafsson, H. Habberstad, and U. Orguner, "Multi-target tracking with PHD filter using Doppler-only measurements," *Digit. Signal Process.*, vol. 27, pp. 1–11, 2014.
[100] N. H. Nguyen and K. Doğançay, "Optimal sensor placement for Doppler shift target localization," in *Proc. IEEE Radar Conf.*, 2015, pp. 1677–1682.
[101] Y. Wang et al., "ISAC enabled cooperative detection for cellular-connected UAV network," *IEEE Trans. Wireless Commun.*, vol. 24, no. 2, pp. 1541–1554, Feb. 2025.
[102] C. Yan, L. Fu, J. Zhang, and J. Wang, "A comprehensive survey on UAV communication channel modeling," *IEEE Access*, vol. 7, pp. 107769–107792, 2019.
[103] S. Jie Seah et al., "Empirical channel models for UAV communication: A comparative study," *IEEE Access*, vol. 12, pp. 96740–96756, 2024.

Jianzhe Xue (Graduate Student Member, IEEE) received the B.S. degree in communication engineering from Xidian University, Xi'an, China, in 2021. He is currently working toward the Ph.D. degree with the School of Electronic Science and Engineering, Nanjing University, Nanjing, China. He was a joint Ph.D. Student with Broadband Communications Research Group, Department of Electrical and Computer Engineering, University of Waterloo, Waterloo, ON, Canada. His research interests include Internet of Vehicles, intelligent signal processing, and machine learning for wireless communications. He was the recipient of the IEEE Daniel E. Noble Fellowship Award.

Haibo Zhou (Fellow, IEEE) received the Ph.D. degree in information and communication engineering from Shanghai Jiao Tong University, Shanghai, China, in 2014. From 2014 to 2017, he was a Postdoctoral Fellow with Broadband Communications Research Group, Department of Electrical and Computer Engineering, University of Waterloo, Waterloo, ON, Canada. He is currently a Full Professor with the School of Electronic Science and Engineering, Nanjing University, Nanjing, China. His research interests include resource management and protocol design in B5G/6G networks, vehicular ad hoc networks, and space-air-ground integrated networks. He was the recipient of the 2019 IEEE ComSoc Asia–Pacific Outstanding Young Researcher Award, 2023 IEEE ComSoc WTC Outstanding Young Researcher Award, 2023-2024 IEEE ComSoc Distinguished Lecturer, and 2023-2025 IEEE VTS Distinguished Lecturer. He served as Track/Symposium Co-Chair of IEEE/CIC ICCC 2019, IEEE VTC-Fall 2020, IEEE VTC-Fall 2021, WCSP 2022, IEEE GLOBECOM 2022, IEEE ICC 2024, and IEEE GLOBECOM 2024. He is an Associate Editor for IEEE TRANSACTIONS ON WIRELESS COMMUNICATIONS, IEEE INTERNET OF THINGS JOURNAL, *IEEE Network Magazine*, and *Journal of Communications and Information Networks*.

Haohai Huang (Student Member, IEEE) received the B.S. degree in communication engineering in 2024 from Nanjing University, Nanjing, China, where he is currently working toward the M.S. degree with the School of Electronic Science and Engineering. His research interests include Internet of Vehicles and wireless communications.

Gui Wen (Student Member, IEEE) received the B.S. degree in transportation construction and equipment from Chang'an University, Xi'an, China, in 2012, and the M.S. degree in automotive engineering (vehicle research, development and production) from the Ilmenau University of Technology, Ilmenau, Germany, in 2018. He is currently working toward the Ph.D. degree with the School of Electronic Science and Engineering, Nanjing University, Nanjing, China. He serves as a Systems Engineer with China Unicom Smart Connection Technology Limited. His research interests include Internet of Vehicles, autonomous driving, and intelligent transportation.

Yunting Xu (Member, IEEE) received the Ph.D degree from Nanjing University, Nanjing, China, in 2024. He is currently a Research Fellow with the School of Computer Science and Engineering, Nanyang Technological University, Singapore. His research focuses on the artificial intelligence and networking optimization in the field of emerging wireless networks.

Xinyu Huang (Member, IEEE) received the B.E. degree from Qian Xuesen Experimental Class, Xidian University, Xi'an, China, in 2018, and the M.S. degree in information and communications engineering from Xi'an Jiaotong University, Xi'an, in 2021, and the Ph.D. degree in electrical and computer engineering from the University of Waterloo, Waterloo, ON, Canada, in 2025. He is currently a Postdoctoral Fellow with the Department of Electrical and Computer Engineering, University of Waterloo. His research interests include digital agents, multimedia communications, ISAC, and network management.

Xuemin Shen (Fellow, IEEE) received the Ph.D. degree in electrical engineering from Rutgers University, New Brunswick, NJ, USA, in 1990. He is currently a University Professor with the Department of Electrical and Computer Engineering, University of Waterloo, Waterloo, ON, Canada. His research interests include network resource management, wireless network security, Internet of Things, 5G and beyond, and vehicular ad hoc and sensor networks. He is a registered Professional Engineer of Ontario, Canada, Engineering Institute of Canada Fellow, Canadian Academy of Engineering Fellow, Royal Society of Canada Fellow, Chinese Academy of Engineering Foreign Member, and Distinguished Lecturer of IEEE Vehicular Technology Society and Communications Society. He was the recipient of the Canadian Award for Telecommunications Research from the Canadian Society of Information Theory (CSIT) in 2021, R.A. Fessenden Award in 2019 from IEEE, Canada, Award of Merit from the Federation of Chinese Canadian Professionals (Ontario) in 2019, James Evans Avant Garde Award in 2018 from the IEEE Vehicular Technology Society, Joseph LoCicero Award in 2015 and Education Award in 2017 from the IEEE Communications Society, and Technical Recognition Award from Wireless Communications Technical Committee (2019), and AHSN Technical Committee (2013). He has also the recipient of the Excellent Graduate Supervision Award in 2006 from the University of Waterloo and the Premiers Research Excellence Award (PREA) in 2003 from the Province of Ontario, Canada. He served as the Technical Program Committee Chair/CoChair of IEEE Globecom 16, IEEE Infocom14, IEEE VTC10 Fall, and IEEE Globecom07, and Chair of IEEE Communications Society Technical Committee on Wireless Communications. He is the President of IEEE Communications Society. He was the Vice President of Technical & Educational Activities, Vice President of Publications, Member-at-Large on the Board of Governors, Chair of Distinguished Lecturer Selection Committee, Member of IEEE Fellow Selection Committee of the ComSoc. He served as the Editor-in-Chief of IEEE INTERNET OF THINGS JOURNAL, IEEE NETWORK, and *IET Communications*.